

On the Dynamics of Navier-Stokes and Euler Equations

Yueheng Lan and Y. Charles Li

ABSTRACT. This is a rather comprehensive study on the dynamics of Navier-Stokes and Euler equations via a combination of analysis and numerics. We focus upon two main aspects: (a). zero viscosity limit of the spectra of linear Navier-Stokes operator, (b). heteroclinics conjecture for Euler equation, its numerical verification, Melnikov integral, and simulation and control of chaos. Besides Navier-Stokes and Euler equations, we also study two models of them.

CONTENTS

1. Introduction	2
2. Zero Viscosity Limit of the Spectrum of 2D Linear Navier-Stokes Operator	4
3. The Heteroclinics Conjecture for 2D Euler Equation	12
4. Numerical Verification of the Heteroclinics Conjecture for 2D Euler Equation	18
5. Melnikov Integral and Numerical Simulation of Chaos in 2D Navier-Stokes Equation	19
6. Melnikov Integral and Control of Chaos in 2D Navier-Stokes Equation	26
7. Zero Viscosity Limit of the Spectrum of 3D Linear Navier-Stokes Operator	28
8. Numerical Verification of the Heteroclinics Conjecture for 3D Euler Equations	35
9. Melnikov Integral and Numerical Simulation of Chaos in 3D Navier-Stokes Equation	37
10. Melnikov Integral and Control of Chaos in 3D Navier-Stokes Equation	41
11. Numerical Verification of the Heteroclinics Conjecture for a Line Model	42
12. Melnikov Integral and Numerical Simulation of Chaos in the Line Model	43
13. Melnikov Integral and Control of Chaos in the Line Model	45
14. Numerical Verification of the Heteroclinics Conjecture for a Two Lines Model	45

1991 *Mathematics Subject Classification*. Primary 35, 37; Secondary 34, 46.

Key words and phrases. Heteroclinic orbit, chaos, turbulence, control, Melnikov integral, zero viscosity limit, sine-Gordon equation, Navier-Stokes equations, Euler equations.

©2006 (copyright holder)

15. Melnikov Integral and Numerical Simulation of Chaos in the Two Lines Model	46
16. Melnikov Integral and Control of Chaos in the Two Lines Model	48
17. Conclusion and Discussion	48
18. Appendix A: Melnikov Integral and Control of Chaos in a Sine-Gordon Equation	50
19. Appendix B: The Lagrange Flow Induced by a Solution to the 2D Euler Equation Is Always Integrable	52
References	52

1. Introduction

The dynamics of Navier-Stokes and Euler equations is a challenging problem. In particular, such dynamics can be chaotic or turbulent. The main challenge comes from the large dimensionality of the phase space where the Navier-Stokes and Euler equations pose extremely intricate flows. Here the dynamics we refer to is the so-called Eulerian, in contrast to the so-called Lagrangian, dynamics of fluids. The Eulerian dynamics is a dynamics in an infinite dimensional phase space (e.g. a Banach space) posed by the Cauchy problem of either the Navier-Stokes or the Euler equations as partial differential equations. The Lagrangian dynamics of fluid particles is a dynamics of a system of two or three ordinary differential equations with vector fields given by fluid velocities. The Lagrangian dynamics of fluid particles in three dimensions can be chaotic even when the Eulerian dynamics is steady (e.g. the ABC flow [2]). Nevertheless, as shown in Appendix B, the Lagrangian dynamics of 2D inviscid fluid particles is always integrable.

Even though the global well-posedness of 3D Navier-Stokes and Euler equations is still an interesting open mathematical problem, 3D Navier-Stokes and Euler equations have local well-posedness which is often enough for a dynamical system study in the phase space. To begin such a dynamical system study, one needs to understand the spectra of the linear Navier-Stokes and/or Euler operators [17]. The spectra of the linear Navier-Stokes operators consist of eigenvalues, whereas the spectra of the linear Euler operators contain continuous spectra. Existence of invariant manifolds can be proved for Navier-Stokes equations [17], but is still open for Euler equations. The size of the invariant manifolds for Navier-Stokes equations tends to zero in the zero viscosity limit [17]. We find that the spectra of the linear Navier-Stokes and Euler operators can be classified into four categories in the zero viscosity limit:

- (1) *Persistence*: These are the eigenvalues that persist and approach to the eigenvalues of the corresponding linear Euler operator when the viscosity approaches zero.
- (2) *Condensation*: These are the eigenvalues that approach and form a continuous spectrum for the corresponding linear Euler operator when the viscosity approaches zero.
- (3) *Singularity*: These are the eigenvalues that approach to a set that is not in the spectrum of the corresponding linear Euler operator when the viscosity approaches zero.

- (4) *Addition:* This is a subset of the spectrum of the linear Euler operator, which has no overlap with the zero viscosity limit set of the spectrum of the linear NS operator.

We also find that as the viscosity approaches zero, the spectrum of the linear Navier-Stokes operator undergoes a fascinating deformation. Focusing upon the persistent unstable eigenvalue, we propose a heteroclinics conjecture, i.e. there should be a heteroclinic orbit (in fact heteroclinic cycles) associating to the instability for Euler equation. We will present both analytical and numerical study upon this heteroclinics conjecture. Then we conduct a Melnikov integral calculation along the numerically obtained approximate heteroclinic orbit. We also compare the Melnikov prediction with the numerical simulation and control of chaos for the Navier-Stokes equations. Numerically we mainly use the Liapunov exponent as a measure of chaos. In some case, we also plot the Poincaré return map. We realize that the size of Galerkin truncations for the full Navier-Stokes equations is limited by the computer ability. Thus we propose two simpler models of the Navier-Stokes equations. For the so-called line model, we obtain numerically exact heteroclinic orbits for any size of Galerkin truncations. We also realize that due to viscosity, the chaos in Galerkin truncations of Navier-Stokes equations is often transient chaos, i.e. the chaos has a finite life time. Infinite life time chaos can be observed in Galerkin truncations of Euler equations.

Chaos and turbulence have no good averages [21]. The matter is more fundamental than just poor understanding of averages. The very mechanism of chaos leads to the impossibility of a good average [16]. On the other hand, chaos and turbulence are ubiquitous. In high dimensional systems, there exists tubular chaos [16] [13] [14] [15] which further confirms that there is no good average. The hope is that chaos and turbulence can be controlled. Two aspects of control are practically important in applications: Taming and enhancing. When an airplane meets turbulence, it will be nice, safer and economic if we can tame the turbulence into a laminar flow or a less turbulent flow [1] [8] [25]. In a combustor, enhancing turbulence can get the fuel and oxidant mixed and burned more efficiently [25] [8]. Theoretically, one can also make use of the ergodicity of chaos to gear an orbit to a specific target [27]. Many other possibilities of applications of control can be designed too. An advantage of the control is that it can be done in a trial-correction manner without a detailed knowledge of turbulence.

Clearly, control of chaos and turbulence has great industrial value. From a mathematical point of view, the question is how much mathematics is in this control theory. So far, the mathematical merit of the theory of control of chaos is not nearly as great as proving the existence of chaos [16]. Obviously, a lot of good numerics is in this control theory. In this article, we will address this control theory from a mathematical perspective, and try to formulate some good mathematical problems. One can add a control to any equation. But the only meaningful controls are the ones that are practical. Consider the 3D Navier-Stokes equations for example

$$u_{i,t} + u_j u_{i,j} = -p_{,i} + \epsilon u_{i,jj} + f_i + \mathcal{C}_i ,$$

defined on a spatial domain \mathcal{D} with appropriate boundary conditions, where $\epsilon = 1/\text{Re}$ is the inverse of the Reynolds number, and $f_i = f_i(t, x)$ is the external force. Assume that without the control \mathcal{C}_i , the solutions are turbulent. The goal is to find

a practical control to either tame or enhance turbulence. For instance, a practical control $\mathcal{C}_i = \mathcal{C}_i(t, x)$ should be spatially localized (perhaps near the boundary).

Recently, there has been quite amount of works on numerical simulations of chaos in Navier-Stokes equations [3] [4] [7] [26] [31] [30]. Here we try to combine numerics with analysis in terms of Melnikov integrals. Unlike the sine-Gordon system studied in Appendix A, analytical calculation of the Melnikov integrals is not feasible at this moment for Navier-Stokes equations. So we will resort to numerical calculations. It is an interesting open mathematical problem that whether or not 2D Euler equation is integrable as a Hamiltonian system in the Liouville sense. Since 2D Euler equation possesses infinitely many constants of motion, it is tempting to conjecture that 2D Euler equation is integrable. Another support to such a conjecture is that both 2D and 3D Euler equations have Lax pairs [11] [23] [20]. In fact, it is even rational to conjecture that 3D Euler equations are integrable. As mentioned above, we propose the so-called heteroclinics conjecture for Euler equations, i.e. there exist heteroclinic cycles for Euler equations. We numerically simulate the heteroclinic orbits and use the numerical results to conduct numerical calculations on Melnikov integrals. In these numerical simulations, it is crucial to make use of known results on the spectra of linear Navier-Stokes and Euler operators [10] [9] [17]. We use the numerical Melnikov integral as a tool for both predicting and controlling chaos. As a measure of chaos, we calculate the Liapunov exponents. We find that the calculated Liapunov exponents depend on the computational time interval and the precision of the computation. Nevertheless, as a measure of chaos, Liapunov exponents prove to be very robust. Since the chaos is often transient, we make comparison on the base of fixed time interval and fixed precision of computation.

Our numerics resorts to Galerkin truncations. But Galerkin truncations are somewhat singular perturbations of Euler equations. Higher single Fourier modes have more unstable eigenvalues. Therefore, it is difficult to derive dynamical pictures for Euler equations from their Galerkin truncations. On the other hand, higher single Fourier modes have more dissipation under Navier-Stokes flows. So Galerkin truncations perform better for Navier-Stokes equations than Euler equations. Today's computer ability still limits the size of the Galerkin truncations. With better future computer ability, Galerkin truncations will paint better and better pictures of Navier-Stokes and Euler equations. It seems also important to design special models that can picture special aspects of the dynamics of Navier-Stokes and Euler equations.

2. Zero Viscosity Limit of the Spectrum of 2D Linear Navier-Stokes Operator

We will study the following form of 2D Navier-Stokes (NS) equation with a control,

$$(2.1) \quad \partial_t \Omega + \{\Psi, \Omega\} = \epsilon[\Delta \Omega + f(t, x) + b\tilde{\delta}(x)] ,$$

where Ω is the vorticity which is a real scalar-valued function of three variables t and $x = (x_1, x_2)$, the bracket $\{ , \}$ is defined as

$$\{f, g\} = (\partial_{x_1} f)(\partial_{x_2} g) - (\partial_{x_2} f)(\partial_{x_1} g) ,$$

where Ψ is the stream function given by,

$$u_1 = -\partial_{x_2}\Psi, \quad u_2 = \partial_{x_1}\Psi,$$

the relation between vorticity Ω and stream function Ψ is,

$$\Omega = \partial_{x_1}u_2 - \partial_{x_2}u_1 = \Delta\Psi,$$

and $\epsilon = 1/\text{Re}$ is the inverse of the Reynolds number, Δ is the 2D Laplacian, $f(t, x)$ is the external force, $b\tilde{\delta}(x)$ is the spatially localized control, and b is the control parameter. We pose the periodic boundary condition

$$\Omega(t, x_1 + 2\pi, x_2) = \Omega(t, x_1, x_2) = \Omega(t, x_1, x_2 + 2\pi/\alpha),$$

where α is a positive constant, i.e. the 2D NS is defined on the 2-torus \mathbb{T}^2 . We require that Ψ , f and $\tilde{\delta}$ have mean zero

$$\int_{\mathbb{T}^2} \Psi dx = \int_{\mathbb{T}^2} f dx = \int_{\mathbb{T}^2} \tilde{\delta} dx = 0.$$

Of course Ω always has zero mean. In this case, $\Psi = \Delta^{-1}\Omega$.

In both 2D and 3D, the linear NS operator obtained by linearizing NS at a fixed point has only point spectrum consisting of eigenvalues lying in a parabolic region [17]. On the other hand, the corresponding linear Euler can have continuous spectrum besides point spectrum [17]. The spectra of the linear NS and Euler operators can be classified into four classes in the zero viscosity limit:

- (1) *Persistence*: These are the eigenvalues that persist and approach to the eigenvalues of the corresponding linear Euler operator when the viscosity approaches zero.
- (2) *Condensation*: These are the eigenvalues that approach and form a continuous spectrum for the corresponding linear Euler operator when the viscosity approaches zero.
- (3) *Singularity*: These are the eigenvalues that approach to a set that is not in the spectrum of the corresponding linear Euler operator when the viscosity approaches zero.
- (4) *Addition*: This is a subset of the spectrum of the linear Euler operator, which has no overlap with the zero viscosity limit set of the spectrum of the linear NS operator.

2.1. A Shear Fixed Point. For the external force $f = \Gamma \cos x_1$ ($b = 0$), $\Omega = \Gamma \cos x_1$ is a shear fixed point, where Γ is an arbitrary real nonzero constant. Choose $\alpha \in (0.5, 0.84)$. There is a $\epsilon_* > 0$ such that when $\epsilon > \epsilon_*$, the fixed point has no eigenvalue with positive real part, and when $\epsilon \in [0, \epsilon_*)$, the fixed point has a unique positive eigenvalue [17]. Notice that this unique eigenvalue persists even for linear Euler ($\epsilon = 0$). In fact, for linear Euler ($\epsilon = 0$), there is a pair of eigenvalues, and the other one is the negative of the above eigenvalue. Precise statements on such results are given in the theorem below. Later we will discover numerically that some of the rest eigenvalues of the linear Navier-Stokes operator somehow form the continuous spectrum of linear Euler ($\epsilon = 0$) as $\epsilon \rightarrow 0$, while others do not converge to the spectrum of linear Euler ($\epsilon = 0$) at all [17] [18]. Using the Fourier series

$$\Omega = \sum_{k \in \mathbb{Z}^2 / \{0\}} \omega_k e^{i(k_1 x_1 + \alpha k_2 x_2)},$$

where $\omega_{-k} = \overline{\omega_k}$ (in fact, we always work in the subspace where all the ω_k 's are real-valued), one gets the spectral equation of the linearized 2D Navier-Stokes operator at the fixed point $\Omega = 2 \cos x_1$,

$$(2.2) \quad A_{n-1}\omega_{n-1} - \epsilon|\hat{k} + np|^2\omega_n - A_{n+1}\omega_{n+1} = \lambda\omega_n ,$$

where $\hat{k} \in \mathbb{Z}^2/\{0\}$, $p = (1, 0)$, $\omega_n = \omega_{\hat{k}+np}$, $A_n = A(p, \hat{k} + np)$, and

$$A(q, r) = \frac{\alpha}{2} \left[\frac{1}{r_1^2 + (\alpha r_2)^2} - \frac{1}{q_1^2 + (\alpha q_2)^2} \right] \begin{vmatrix} q_1 & r_1 \\ q_2 & r_2 \end{vmatrix} .$$

(In fact, the A_n 's should be counted twice due to switching q and r , but the difference is only a simple scaling of ϵ and λ .) Thus the 2D linear NS decouples according to lines labeled by \hat{k} . The following detailed theorem on the spectrum of the 2D linear NS at the fixed point $\Omega = 2 \cos x_1$ was proved in [17].

Theorem 2.1 (The Spectral Theorem [17]). *The spectra of the 2D linear NS operator (2.2) have the following properties.*

- (1) $(\alpha\hat{k}_2)^2 + (\hat{k}_1 + n)^2 > 1$, $\forall n \in \mathbb{Z}/\{0\}$. When $\epsilon > 0$, there is no eigenvalue of non-negative real part. When $\epsilon = 0$, the entire spectrum is the continuous spectrum

$$\left[-i\alpha|\hat{k}_2|, i\alpha|\hat{k}_2| \right] .$$

- (2) $\hat{k}_2 = 0$, $\hat{k}_1 = 1$. The spectrum consists of the eigenvalues

$$\lambda = -\epsilon n^2, \quad n \in \mathbb{Z}/\{0\} .$$

The eigenfunctions are the Fourier modes

$$\tilde{\omega}_{np} e^{inx_1} + c.c. , \quad \forall \tilde{\omega}_{np} \in \mathcal{C} , \quad n \in \mathbb{Z}/\{0\} .$$

As $\epsilon \rightarrow 0^+$, the eigenvalues are dense on the negative half of the real axis $(-\infty, 0]$. Setting $\epsilon = 0$, the only eigenvalue is $\lambda = 0$ of infinite multiplicity with the same eigenfunctions as above.

- (3) $\hat{k}_2 = -1$, $\hat{k}_1 = 0$. (a). $\epsilon > 0$. For any $\alpha \in (0.5, 0.95)$, there is a unique $\epsilon_*(\alpha)$,

$$(2.3) \quad \frac{\sqrt{32 - 3\alpha^6 - 17\alpha^4 - 16\alpha^2}}{2(\alpha^2 + 1)(\alpha^2 + 4)} < \epsilon_*(\alpha) < \frac{1}{(\alpha^2 + 1)} \sqrt{\frac{1 - \alpha^2}{2}} ,$$

where the term under the square root on the left is positive for $\alpha \in (0.5, 0.95)$, and the left term is always less than the right term. When $\epsilon > \epsilon_*(\alpha)$, there is no eigenvalue of non-negative real part. When $\epsilon = \epsilon_*(\alpha)$, $\lambda = 0$ is an eigenvalue, and all the rest eigenvalues have negative real parts. When $\epsilon < \epsilon_*(\alpha)$, there is a unique positive eigenvalue $\lambda(\epsilon) > 0$, and all the rest eigenvalues have negative real parts. $\epsilon^{-1}\lambda(\epsilon)$ is a strictly monotonically decreasing function of ϵ . When $\alpha \in (0.5, 0.8469)$, we have the estimate

$$\begin{aligned} & \sqrt{\frac{\alpha^2(1 - \alpha^2)}{2(\alpha^2 + 1)} - \frac{\alpha^4(\alpha^2 + 3)}{4(\alpha^2 + 1)(\alpha^2 + 4)}} - \epsilon(\alpha^2 + 1) < \lambda(\epsilon) \\ & < \sqrt{\frac{\alpha^2(1 - \alpha^2)}{2(\alpha^2 + 1)}} - \epsilon\alpha^2 , \end{aligned}$$

where the term under the square root on the left is positive for $\alpha \in (0.5, 0.8469)$.

$$\sqrt{\frac{\alpha^2(1-\alpha^2)}{2(\alpha^2+1)} - \frac{\alpha^4(\alpha^2+3)}{4(\alpha^2+1)(\alpha^2+4)}} \leq \lim_{\epsilon \rightarrow 0^+} \lambda(\epsilon) \leq \sqrt{\frac{\alpha^2(1-\alpha^2)}{2(\alpha^2+1)}}.$$

In particular, as $\epsilon \rightarrow 0^+$, $\lambda(\epsilon) = \mathcal{O}(1)$.

(b). $\epsilon = 0$. When $\alpha \in (0.5, 0.8469)$, we have only two eigenvalues λ_0 and $-\lambda_0$, where λ_0 is positive,

$$\sqrt{\frac{\alpha^2(1-\alpha^2)}{2(\alpha^2+1)} - \frac{\alpha^4(\alpha^2+3)}{4(\alpha^2+1)(\alpha^2+4)}} < \lambda_0 < \sqrt{\frac{\alpha^2(1-\alpha^2)}{2(\alpha^2+1)}}.$$

The rest of the spectrum is a continuous spectrum $[-i\alpha, i\alpha]$.

(c). For any fixed $\alpha \in (0.5, 0.8469)$,

$$(2.4) \quad \lim_{\epsilon \rightarrow 0^+} \lambda(\epsilon) = \lambda_0.$$

(4) Finally, when $\epsilon = 0$, the union of all the above pieces of continuous spectra is the imaginary axis $i\mathbb{R}$.

Remark 2.2. In the current periodic boundary condition case, viscosity does not destabilize the flow in contrast to the non-slip boundary condition case [24]. The Orr-Sommerfeld equation and Rayleigh equation have the same periodic boundary condition in the former case, and different number of boundary conditions in the latter case.

The following invariant manifold theorem of the 2D NS at the fixed point $\Omega = 2 \cos x_1$ was also proved in [17].

Theorem 2.3 (Invariant Manifold Theorem [17]). *For any $\alpha \in (0.5, 0.95)$, and $\epsilon \in (0, \epsilon_*(\alpha))$ where $\epsilon_*(\alpha) > 0$ satisfies (2.3), in a neighborhood of $\Omega = 2 \cos x_1$ in the Sobolev space $H^\ell(\mathbb{T}^2)$ ($\ell \geq 3$), there are an 1-dimensional C^∞ unstable manifold and an 1-codimensional C^∞ stable manifold.*

One of the goals of the work [17] is to study the zero viscosity limit of the invariant manifolds of the 2D NS. For this study, it is crucial to understand the deformation of the linear spectra as $\epsilon \rightarrow 0^+$. Below we will study this numerically.

When $\hat{k}_1 = 0$ and $\hat{k}_2 = 1$, $\alpha = 0.7$, the unique ϵ_* in (2.3) belongs to the interval $0.332 < \epsilon_* < 0.339$, such that when $\epsilon < \epsilon_*$, a positive eigenvalue appears. We test this criterion numerically and find that it is very sharp even when the truncation of the linear system (2.2) is as low as $|n| \leq 100$. As $\epsilon \rightarrow 0^+$, we tested the truncation of the linear system (2.2) up to $|n| \leq 1024$ for $\alpha = 0.7$, the patterns are all the same. Below we present the case $|n| \leq 200$ for which the pattern is more clear.

Figure 1 shows the case $\epsilon = 0.14$ where there is one positive eigenvalue and all the rest eigenvalues are negative. Figure 2 shows the case $\epsilon = 0.13$ where a pair of eigenvalues jumps off the real axis and becomes a complex conjugate pair. Figure 3 shows the case $\epsilon = 0.07$ where another pair of eigenvalues jumps off the real axis and becomes a complex conjugate pair. Figure 4 shows the case $\epsilon = 0.03$ where another pair of eigenvalues jumps off the real axis and becomes a complex conjugate pair, while the former two pairs getting closer to each other. Figure 5 shows the case $\epsilon = 0.0004$ where many pairs of eigenvalues have jumped off the real axis and

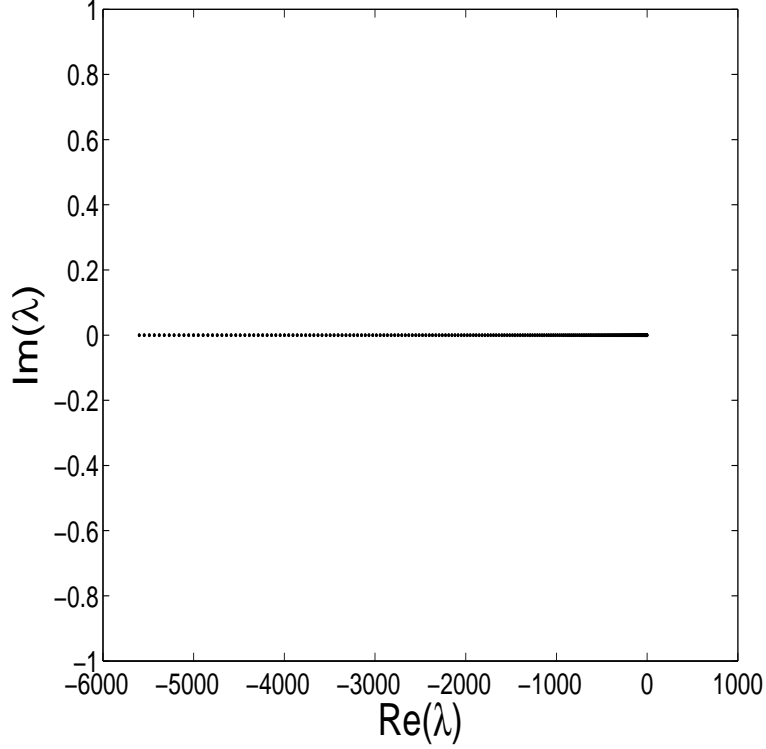


FIGURE 1. The eigenvalues of the linear system (2.2) when $\hat{k}_1 = 0$ and $\hat{k}_2 = 1$, $\alpha = 0.7$, and $\epsilon = 0.14$.

a bubble is formed. Figure 6 shows the case $\epsilon = 0.00013$ where the bubble has expanded. As $\epsilon \rightarrow 0^+$, the limiting picture is shown in Figure 7. Setting $\epsilon = 0$, the spectrum of the line $\hat{k}_1 = 0$ and $\hat{k}_2 = 1$ of the linear Euler operator is shown in Figure 8, where the segment on the imaginary axis is the continuous spectrum. Comparing Figures 7 and 8, we see that the two eigenvalues represent “persistence”, the vertical segment represents “condensation”, and the two horizontal segments represent “singularity”. Next we study one more line: $\hat{k}_1 = 0$ and $\hat{k}_2 = 2$ ($\alpha = 0.7$). In this case, there is no unstable eigenvalue. Figure 9 shows the case $\epsilon = 1.5$ where all the eigenvalues are negative. As ϵ is decreased, the eigenvalues go through the same process of jumping off the real axis and developing a bubble. Figure 10 shows the case $\epsilon = 0.00025$ where the bubble has expanded. As $\epsilon \rightarrow 0^+$, the limiting picture is similar to Figure 7 except that there is no persistent eigenvalue. The cases $\hat{k}_1 = 0$ and $\hat{k}_2 > 2$ ($\alpha = 0.7$) are all the same with the case $\hat{k}_1 = 0$ and $\hat{k}_2 = 2$ ($\alpha = 0.7$). Figure 11 shows the limiting picture of the entire spectrum of the linear NS operator as $\epsilon \rightarrow 0^+$. Figure 12 shows the entire spectrum of the linear Euler operator ($\epsilon = 0$).

The fascinating deformation of the spectra as $\epsilon \rightarrow 0^+$ and the limiting spectral picture clearly depict the nature of singular limit of the spectra as $\epsilon \rightarrow 0^+$. In the “singularity” part of the limit, there is a discrete set of values for the imaginary parts of the eigenvalues, which represent decaying oscillations with a discrete set of

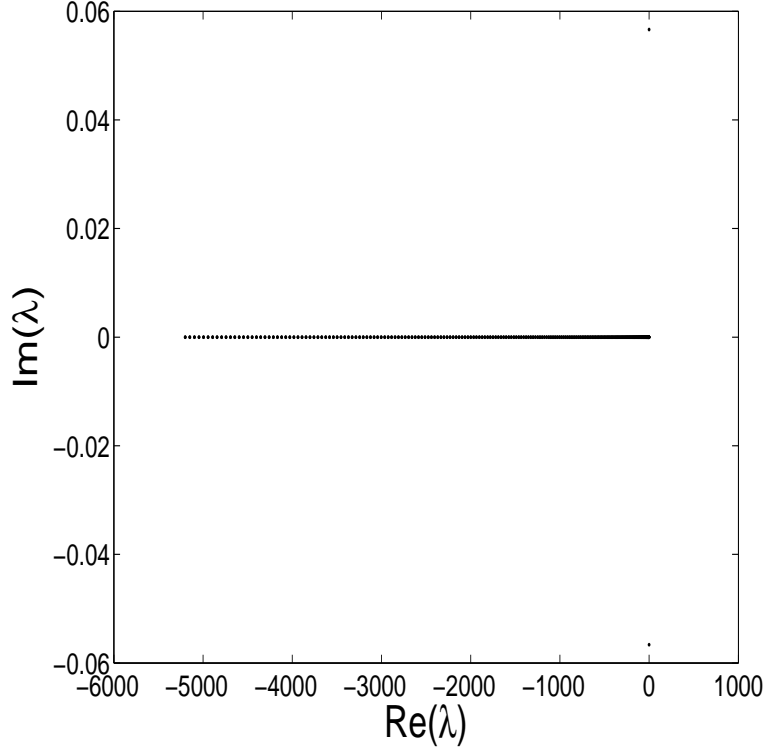


FIGURE 2. The eigenvalues of the linear system (2.2) when $\hat{k}_1 = 0$ and $\hat{k}_2 = 1$, $\alpha = 0.7$, and $\epsilon = 0.13$.

frequencies. Overall, the “singularity” part represents the temporally irreversible nature of the $\epsilon \rightarrow 0^+$ limit, in contrast to the reversible nature of the linear Euler equation ($\epsilon = 0$).

2.2. A Cat’s Eye Fixed Point. In this subsection, we will study another important fixed point – a cat’s eye fixed point. The periodic domain now is the square, i.e. $\alpha = 1$ (instead of 0.7). The cat’s eye fixed point in physical variable is given by

$$(2.5) \quad \Omega = 2 \cos mx_1 + 2\gamma \cos mx_2 ,$$

where m is a positive integer, and $\gamma \in (0, 1]$. In terms of Fourier modes: Let $p = (m, 0)$ and $q = (0, m)$, then the cat’s eye is given by

$$\omega_p^* = 1, \quad \omega_{-p}^* = 1, \quad \omega_q^* = \gamma, \quad \omega_{-q}^* = \gamma ,$$

and all other ω_k^* ’s are zero. The spectral equation for the linear 2D NS operator at the Cat’s eye is then given by

$$(2.6) \quad \begin{aligned} \lambda \omega_k &= A(p, k-p)\omega_{k-p} - A(p, k+p)\omega_{k+p} - \epsilon|k|^2\omega_k \\ &+ \gamma A(q, k-q)\omega_{k-q} - \gamma A(q, k+q)\omega_{k+q} , \end{aligned}$$

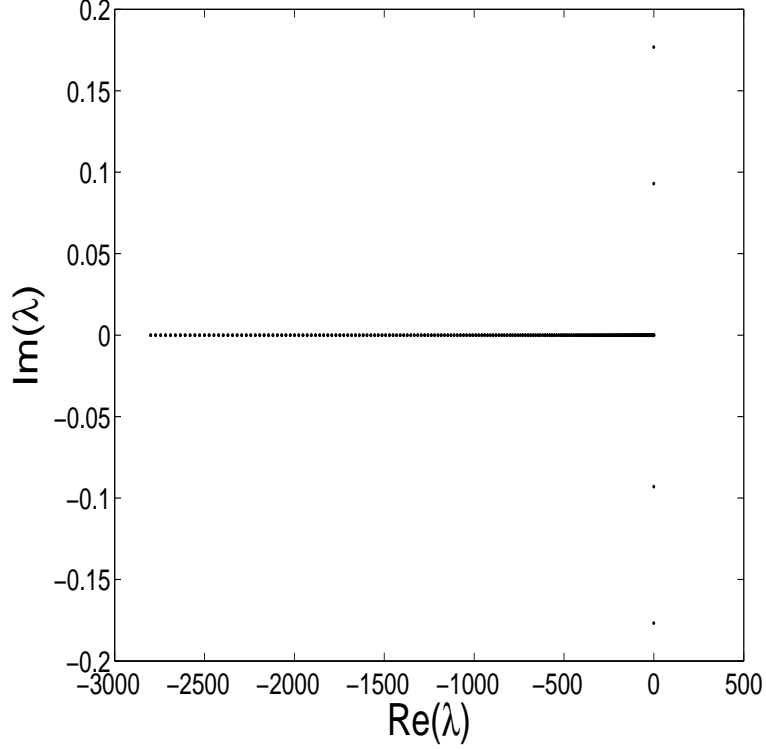


FIGURE 3. The eigenvalues of the linear system (2.2) when $\hat{k}_1 = 0$ and $\hat{k}_2 = 1$, $\alpha = 0.7$, and $\epsilon = 0.07$.

where

$$A(k, r) = \left[\frac{1}{r_1^2 + r_2^2} - \frac{1}{k_1^2 + k_2^2} \right] \begin{vmatrix} k_1 & r_1 \\ k_2 & r_2 \end{vmatrix}.$$

First we study the case of $m = 1$ and $\gamma = 0.5$. Changing the value of γ does not affect the deformation patterns of the eigenvalues of the linear NS (2.6) as $\epsilon \rightarrow 0^+$. We truncate the system (2.6) via the Galerkin truncation $|k_1| \leq 32$ and $|k_2| \leq 32$. This is the largest Galerkin truncation that we are able to compute in a reasonable time. For smaller Galerkin truncations, the deformation patterns of the eigenvalues are the same. When $\epsilon = 150$, all the eigenvalues of the linear NS (2.6) are negative as shown in Figure 13. When ϵ is decreased to $\epsilon = 120$, a pair of eigenvalues jumps off the real axis as shown in Figure 14. When ϵ is decreased to $\epsilon = 80$, three pairs of eigenvalues jump off the real axis as shown in Figure 15. When ϵ is decreased to $\epsilon = 10$, many pairs of eigenvalues have jumped off the real axis and form several parabolas as shown in Figure 16. When ϵ is decreased to $\epsilon = 1$, many parabolas are formed as shown in Figure 17. The $\epsilon \rightarrow 0^+$ limiting picture of the eigenvalues of the linear NS (2.6) is that the eigenvalues are dense on the entire left half plane as shown in Figure 18. The continuous spectrum of the linear Euler, i.e. $\epsilon = 0$ in (2.6), in any Sobolev space $H^s(\mathbb{T}^2)$ where s is a non-negative integer, is a vertical band of width $2s\sigma$ symmetric with respect to the imaginary axis $\{\lambda : |\operatorname{Re}(\lambda)| \leq s\sigma\}$ as shown in Figure 19, where $\sigma > 0$ is the

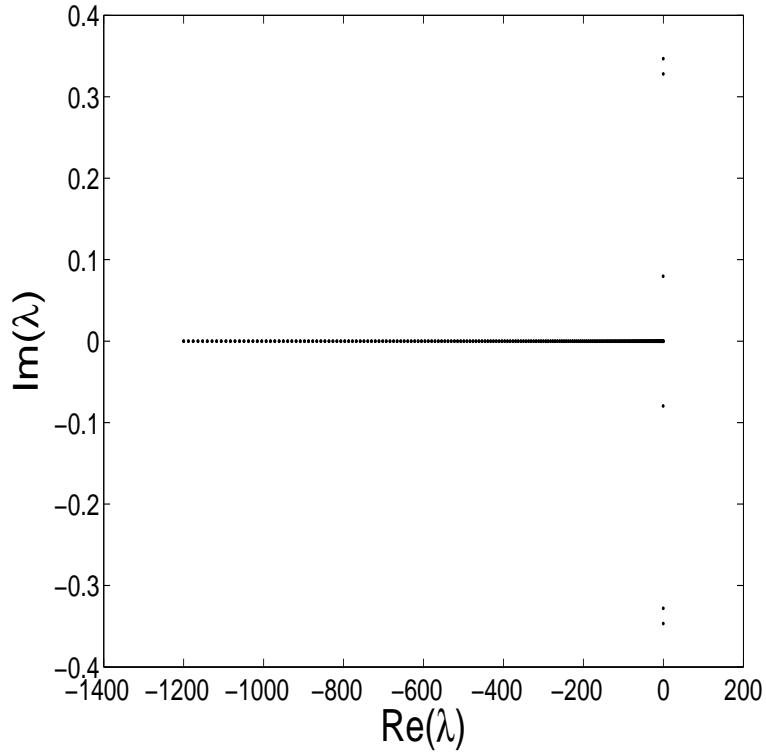


FIGURE 4. The eigenvalues of the linear system (2.2) when $\hat{k}_1 = 0$ and $\hat{k}_2 = 1$, $\alpha = 0.7$, and $\epsilon = 0.03$.

largest Liapunov exponent of the vector field given by the cat's eye (2.5) [29]. Thus the width of the vertical band is proportional to the scale s of the Sobolev space $H^s(\mathbb{T}^2)$. The union of all such bands for all integers $s \geq 0$ is the entire complex plane. The eigenfunctions of the linear NS (2.6) when $\epsilon > 0$ belong to $H^s(\mathbb{T}^2)$ for all integers $s \geq 0$. All the eigenvalues of the linear NS (2.6) condense into the entire left half plane – “condensation”. The right half plane (or right half of the vertical band corresponding to $H^s(\mathbb{T}^2)$) represents “addition”. Thus the possible instability hinted by the right half band of the continuous spectrum of linear Euler in $H^s(\mathbb{T}^2)$ can not be realized by real viscous fluids.

Next we study the case of $m = 2$ and $\gamma = 0.5$. Changing the value of γ does not affect the deformation patterns of the eigenvalues of the linear NS (2.6) as $\epsilon \rightarrow 0^+$. We truncate the system (2.6) via the Galerkin truncation $|k_1| \leq 32$ and $|k_2| \leq 32$. We increase the value of ϵ up to 2×10^4 , there are still eigenvalues with nonzero imaginary parts. These eigenvalues seem always complex no matter how large is ϵ . The imaginary parts of these eigenvalues are unchanged between $\epsilon = 2 \times 10^4$ and $\epsilon = 800$ as can be seen from Figures 20 and 21. Decreasing ϵ , the deformation patterns are similar to those of $m = 1$. When $\epsilon = 0.2$, many eigenvalues have jumped off the real axis and form a dense parabolic region as shown in Figure 22. Decreasing ϵ further, 6 eigenvalues with positive real parts appear, two of which are real, and the rest four are complex. The limiting picture of the spectrum of

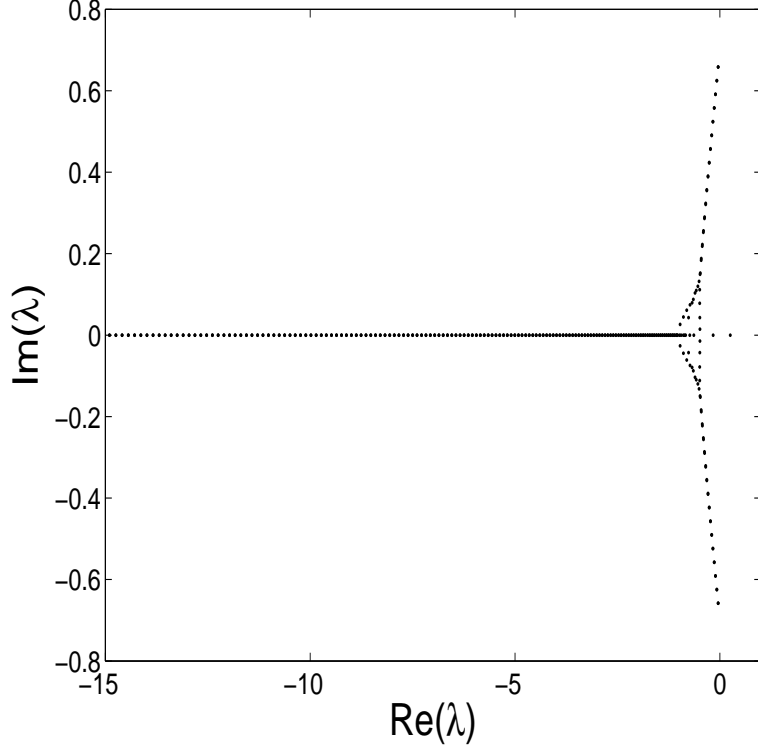


FIGURE 5. The eigenvalues of the linear system (2.2) when $\hat{k}_1 = 0$ and $\hat{k}_2 = 1$, $\alpha = 0.7$, and $\epsilon = 0.0004$.

the linear NS operator (2.6) as $\epsilon \rightarrow 0$ is the same with the $m = 1$ case as shown in Figure 18 except the extra six unstable eigenvalues. The continuous spectrum of the linear Euler operator (2.6) where $\epsilon = 0$ is the same with the $m = 1$ case as shown in Figure 19. There is no analytical result on the eigenvalues of the linear Euler operator (2.6) where $\epsilon = 0$. The numerics indicates that the 6 eigenvalues in the right half plane and other 6 eigenvalues in the left half plane, of the linear NS operator (2.6) persist as $\epsilon \rightarrow 0$, and result in 6 eigenvalues in the right half plane and their negatives for the linear Euler operator (2.6) where $\epsilon = 0$.

3. The Heteroclinics Conjecture for 2D Euler Equation

Setting $\epsilon = 0$ in the 2D Navier-Stokes equation (2.1), one gets the corresponding 2D Euler equation for which one has the following constants of motion:

$$\int_{\mathbb{T}^2} |u|^2 dx, \quad \int_{\mathbb{T}^2} F(\Omega) dx$$

where F is an arbitrary function. Consider the simple fixed point $\Omega = \Gamma \cos x_1$ ($\Gamma \neq 0$ real constant). It has one unstable and one stable real eigenvalues which are negative of each other. The rest of the spectrum is the entire imaginary axis

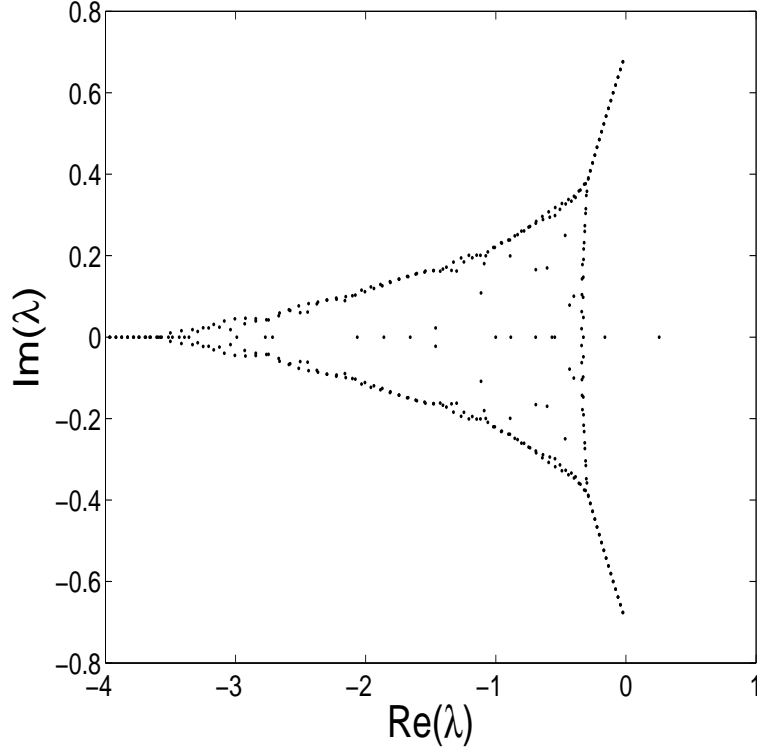


FIGURE 6. The eigenvalues of the linear system (2.2) when $\hat{k}_1 = 0$ and $\hat{k}_2 = 1$, $\alpha = 0.7$, and $\epsilon = 0.00013$.

which is a continuous spectrum [10] [17]. We will use the constant of motion

$$G = \int_{\mathbb{T}^2} \Omega^2 dx - \int_{\mathbb{T}^2} |u|^2 dx$$

to build a Melnikov integral for the corresponding 2D Navier-Stokes equation (2.1). We will try to make use of the Melnikov integral as a measure of chaos and to conduct a control of chaos, around the line of fixed points $\Omega = \Gamma \cos x_1$ parametrized by Γ . G is a linear combination of the kinetic energy and the enstrophy. The gradient of G in Ω is given by

$$\nabla_{\Omega} G = 2(\Omega + \Delta^{-1}\Omega)$$

which is zero along the line of fixed points $\Omega = \Gamma \cos x_1$. We define the Melnikov integral for the 2D NS (2.1) as

$$\begin{aligned} (3.1) \quad M &= \frac{\alpha}{8\pi^2} \int_{-\infty}^{+\infty} \int_{\mathbb{T}^2} \nabla_{\Omega} G[\Delta\Omega + f(t, x) + b\tilde{\delta}(x)] dx dt \\ &= M_0 + bM_c, \end{aligned}$$

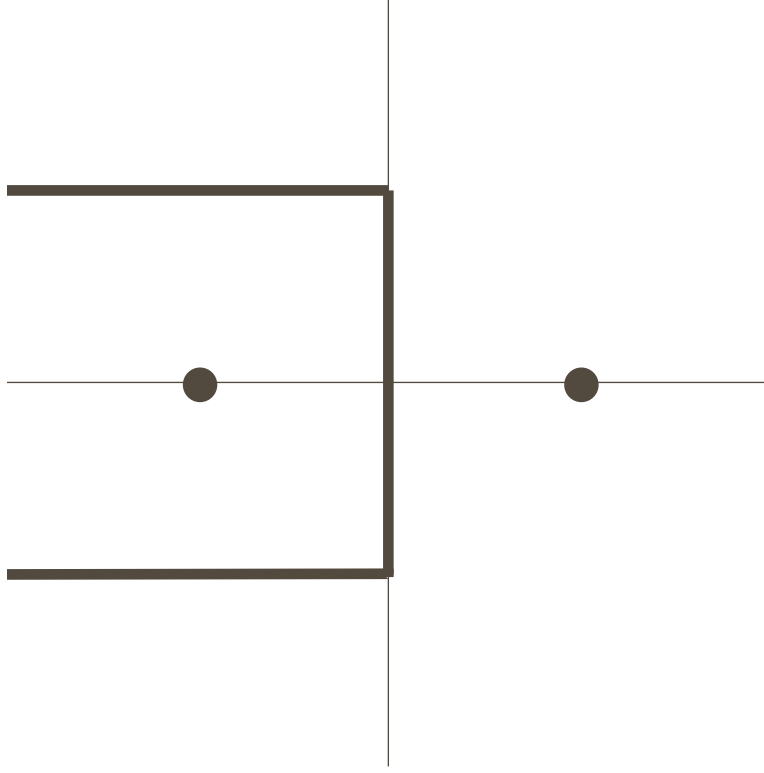


FIGURE 7. The $(\epsilon \rightarrow 0^+)$ limiting picture of the eigenvalues of the linear system (2.2) when $\hat{k}_1 = 0$ and $\hat{k}_2 = 1$, and $\alpha = 0.7$.

where

$$M_0 = \frac{\alpha}{4\pi^2} \int_{-\infty}^{+\infty} \int_{\mathbb{T}^2} (\Omega + \Delta^{-1}\Omega)[\Delta\Omega + f(t, x)] dx dt ,$$

$$M_c = \frac{\alpha}{4\pi^2} \int_{-\infty}^{+\infty} \int_{\mathbb{T}^2} (\Omega + \Delta^{-1}\Omega)\tilde{\delta}(x) dx dt .$$

The question is: Where do we evaluate M ? We propose the following conjecture.

- The Heteroclinics Conjecture: There is a heteroclinic orbit of the 2D Euler equation that connects $\Omega = \Gamma \cos x_1$ and $-\Omega$.

The rationality of this conjecture has been discussed in the Introduction. If this conjecture is true, we can evaluate M along the heteroclinic orbit. Also, under the perturbation of the ϵ term, the heteroclinic orbits may break and re-connect somewhere, thereby generating the heteroclinic chaos. In Appendix A, we show that one can use a Melnikov integral as a criterion to rigorously prove the existence chaos, and to conduct control of chaos. In the current case of 2D NS, the phase space is much more complicated. We do not expect the above Melnikov integral to be a rigorous measure of chaos, rather we believe that it is still relevant to chaos and control of chaos. In fact, often the chaos in 2D NS is a transient chaos. In general, the zeros of a Melnikov integral do not immediately imply the existence of heteroclinic or homoclinic chaos, rather they imply the intersections of the broken

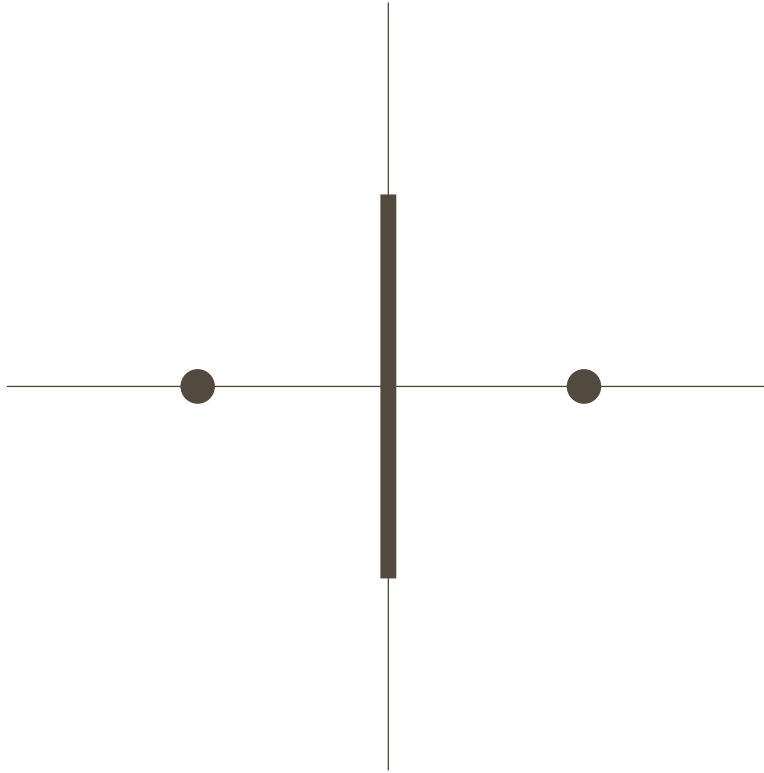


FIGURE 8. The spectrum of the linear system (2.2) when $\epsilon = 0$, $\hat{k}_1 = 0$ and $\hat{k}_2 = 1$, and $\alpha = 0.7$.

heteroclinic orbit with certain center-stable manifold [16]. In fact, the Melnikov integral represents the leading order distance between the broken heteroclinic orbit and the center-stable manifold [16]. Here for 2D NS, rigorous justification even on the above claim is an open problem due to the fact that existence of invariant manifolds for 2D Euler is an open problem.

The 2D Euler equation has several symmetries:

- (1) $\Omega(t, x_1, x_2) \rightarrow \Omega(t, -x_1, -x_2)$,
- (2) $\Omega(t, x_1, x_2) \rightarrow -\Omega(-t, x_1, x_2)$,
- (3) $\Omega(t, x_1, x_2) \rightarrow -\Omega(t, -x_1, x_2)$, or $\Omega(t, x_1, x_2) \rightarrow -\Omega(t, x_1, -x_2)$,
- (4) $\Omega(t, x_1, x_2) \rightarrow \Omega(t, x_1 + \theta_1, x_2 + \theta_2)$, $\forall \theta_1, \theta_2$.

The first symmetry allows us to work in an invariant subspace in which all the ω_k 's are real-valued. This corresponds to the cosine transform in (3.2). In this paper, we will always work in the invariant subspace where all the ω_k 's are real-valued. The second symmetry maps the unstable manifold of $\Gamma \cos x_1$ into the stable manifold of $-\Gamma \cos x_1$. The third symmetry maps the unstable manifold of $\Gamma \cos x_1$ into the unstable manifold of $-\Gamma \cos x_1$. By choosing $\theta_1 = \pi$, the fourth symmetry maps the unstable manifold of $\Gamma \cos x_1$ into the unstable manifold of $-\Gamma \cos x_1$. To maintain the cosine transform, the θ_1 and θ_2 in the fourth symmetry can only be π and π/α .

If the heteroclinics conjecture is true, there is in fact a pair of heteroclinic cycles due to the above symmetries. Indeed, if there is a heteroclinic orbit asymptotic to

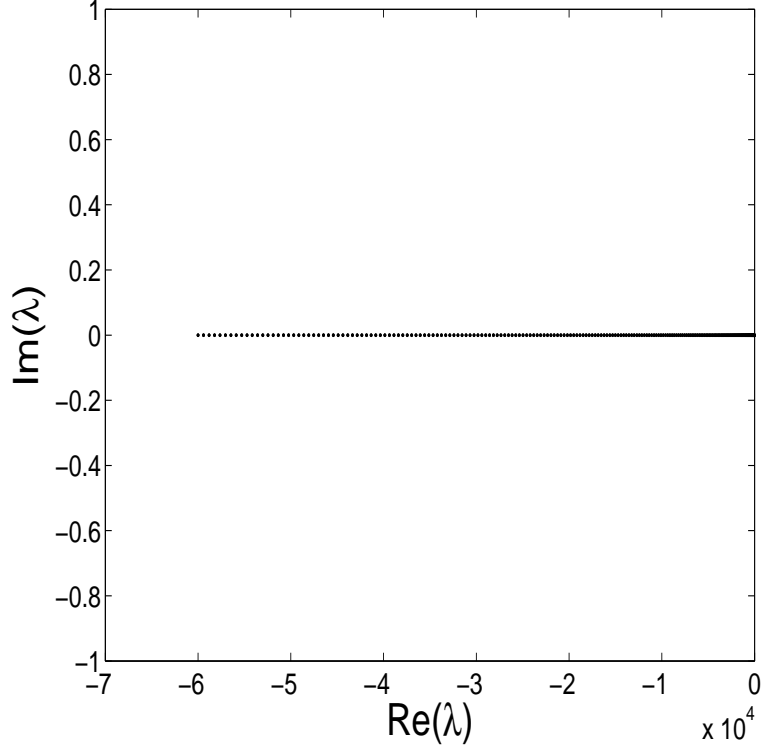


FIGURE 9. The eigenvalues of the linear system (2.2) when $\hat{k}_1 = 0$ and $\hat{k}_2 = 2$, $\alpha = 0.7$, and $\epsilon = 1.5$.

$\Gamma \cos x_1$ and $-\Gamma \cos x_1$ as $t \rightarrow -\infty$ and $+\infty$, then the third symmetry generates another heteroclinic orbit asymptotic to $-\Gamma \cos x_1$ and $\Gamma \cos x_1$ as $t \rightarrow -\infty$ and $+\infty$. Together they form a heteroclinic cycle. Finally the second symmetry generates another heteroclinic cycle. That is, we have a pair of heteroclinic cycles.

Using the Fourier series

$$(3.2) \quad \Omega = \sum_{k \in \mathbb{Z}^2 / \{0\}} \omega_k e^{i(k_1 x_1 + \alpha k_2 x_2)},$$

where $\omega_{-k} = \overline{\omega_k}$ and $F_{-k} = \overline{F_k}$, one gets the kinetic form of the 2D Euler equation

$$\dot{\omega}_k = \sum_{k=m+n} A(m, n) \omega_m \omega_n,$$

where

$$A(m, n) = \frac{\alpha}{2} \left[\frac{1}{n_1^2 + (\alpha n_2)^2} - \frac{1}{m_1^2 + (\alpha m_2)^2} \right] \begin{vmatrix} m_1 & n_1 \\ m_2 & n_2 \end{vmatrix}.$$

Denote by Σ the hyperplane

$$\Sigma = \{\omega \mid \omega_k = 0, \quad \forall \text{ even } k_2\}.$$

Notice that the existence of invariant manifolds around the fixed point $\Omega = \Gamma \cos x_1$ is an open problem. We have the following theorem.

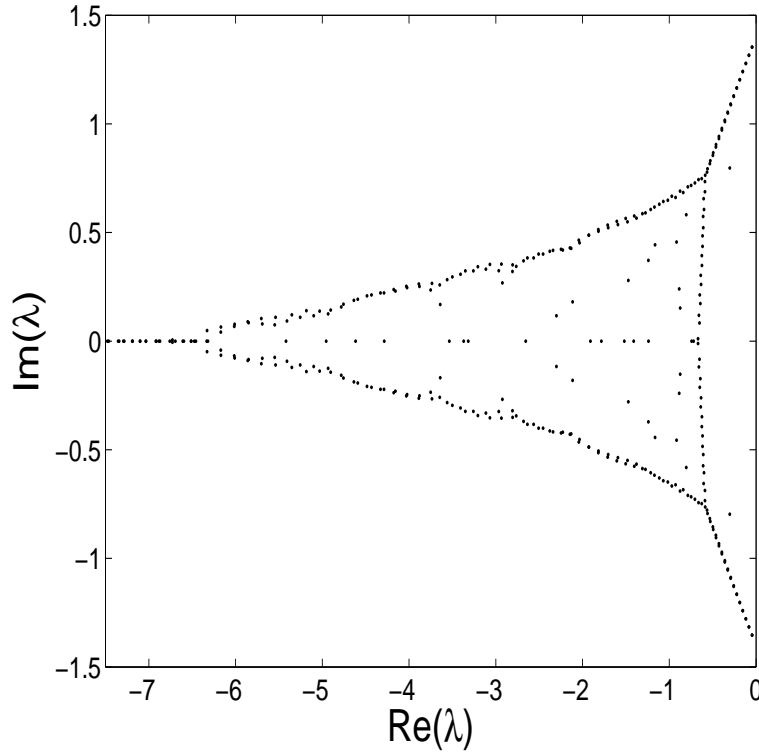


FIGURE 10. The eigenvalues of the linear system (2.2) when $\hat{k}_1 = 0$ and $\hat{k}_2 = 2$, $\alpha = 0.7$, and $\epsilon = 0.00025$.

Theorem 3.1. *Assume that the fixed point $\Omega = \Gamma \cos x_1$ has a 1-dimensional local unstable manifold W^u , and $W^u \cap \Sigma \neq \emptyset$; then the heteroclinics conjecture is true, i.e. there is a heteroclinic orbit to the 2D Euler equation that connects $\Omega = \Gamma \cos x_1$ and $-\Omega$.*

PROOF. Let $\Omega(t, x_1, x_2)$ be an orbit in W^u parametrized such that

$$\Omega(0, x_1, x_2) \in \Sigma .$$

Then by the definition of Σ ,

$$(3.3) \quad \Omega(0, x_1, x_2) = -\Omega(0, x_1, x_2 + \pi/\alpha) .$$

By the second and fourth symmetries,

$$-\Omega(-t, x_1, x_2 + \pi/\alpha)$$

is in the stable manifold of $-\Omega$. Thus

$$\Omega(t, x_1, x_2) \text{ and } -\Omega(-t, x_1, x_2 + \pi/\alpha)$$

are connected at $t = 0$, and together they form a heteroclinic orbit that connects $\Omega = \Gamma \cos x_1$ and $-\Omega$. \square

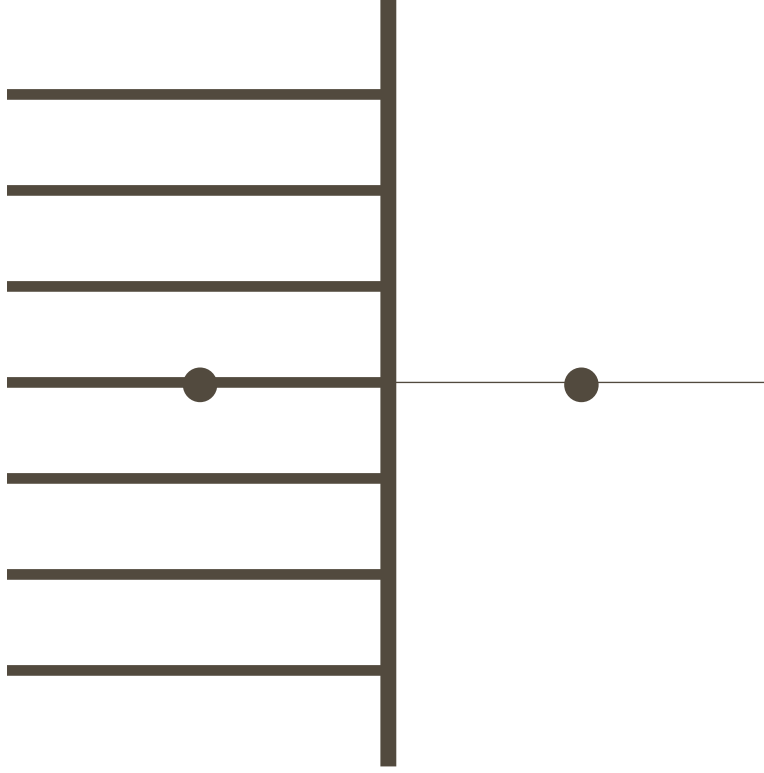


FIGURE 11. The $(\epsilon \rightarrow 0^+)$ limiting picture of the entire spectrum of the linear NS operator (2.2) when $\alpha = 0.7$.

4. Numerical Verification of the Heteroclinics Conjecture for 2D Euler Equation

Besides the symmetries mentioned in last section, we will also make use of the conserved quantities: kinetic energy $E = \sum |k|^{-2} \omega_k^2$ (where $|k|^2 = k_1^2 + \alpha^2 k_2^2$) and enstrophy $S = \sum \omega_k^2$, which will survive as conserved quantities for any symmetric Galerkin truncation, to help us to track the heteroclinic orbit. We will only consider the case that all the ω_k 's are real-valued (i.e. cos-transform).

We make a Galerkin truncation by keeping modes: $\{|k_1| \leq 2, |k_2| \leq 2\}$, which results in a 12 dimensional system. We choose $\alpha = 0.7$. After careful consideration of the above mentioned symmetries and conserved quantities ($E = S = 1$), we discover the following initial condition that best tracks the heteroclinic orbit:

$$(4.1) \quad \begin{aligned} \omega_{(j,0)} = \omega_{(j,2)} = 0, \quad \forall j, \\ \omega_{(0,1)} = 0.603624, \quad \omega_{(1,1)} = -\omega_{(-1,1)} = 0.357832, \\ \omega_{(2,1)} = \omega_{(-2,1)} = 0.435632. \end{aligned}$$

Starting from this initial condition, we calculate the solution in both forward and backward time for the same duration of $T = 11.8$, and we discover the approximate heteroclinic orbit asymptotic to $2 \cos x_1$ and $-2 \cos x_1$ as $t \rightarrow -\infty$ and $+\infty$, as shown in Figure 23. Then the third symmetry generates another heteroclinic orbit

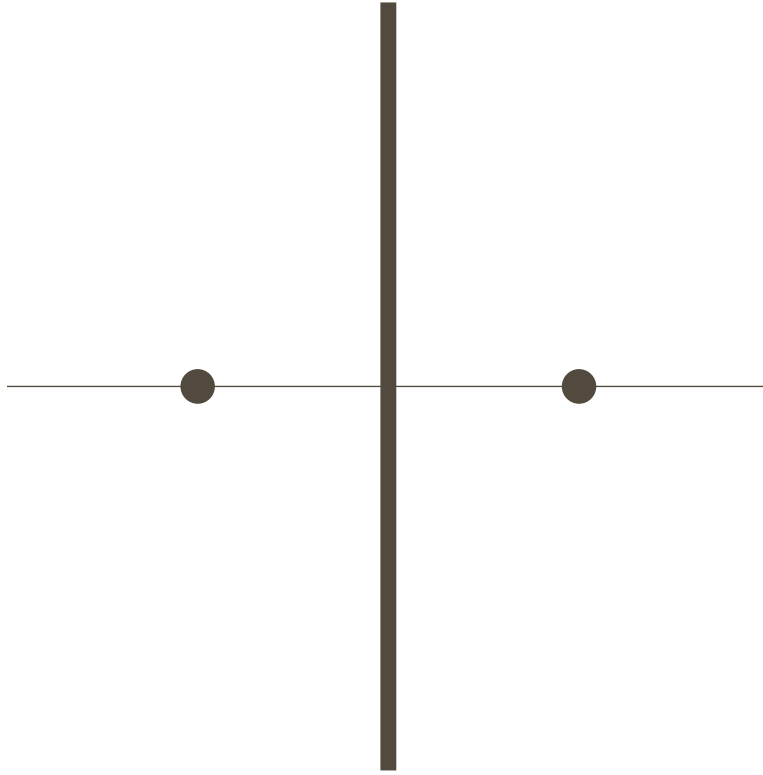


FIGURE 12. The spectrum of the linear Euler operator (2.2) where $\epsilon = 0$ and $\alpha = 0.7$.

asymptotic to $-2 \cos x_1$ and $2 \cos x_1$ as $t \rightarrow -\infty$ and $+\infty$. Together they form a heteroclinic cycle. Finally the second symmetry generates another heteroclinic cycle. That is, we have a pair of heteroclinic cycles. Notice also that the approximate heteroclinic orbit in Figure 23 has an extra loop before landing near $-2 \cos x_1$. This is due to the $k_2 = 2$ modes in the Galerkin truncation. For smaller Galerkin truncations, the heteroclinic orbits can be calculated exactly by hand and have no such extra loop [12] [22], and existence of chaos generated by the heteroclinic orbit can be rigorously proved in some case [22].

Remark 4.1. We have also conducted numerical experiments on Galerkin truncations by keeping more modes: $\{|k_1| \leq 4, |k_2| \leq 4\}$ and $\{|k_1| \leq 8, |k_2| \leq 8\}$. We found orbits that have similar behavior as the approximate heteroclinic orbit in Figure 23, but their approximations to heteroclinics are not as good as the one in Figure 23.

5. Melnikov Integral and Numerical Simulation of Chaos in 2D Navier-Stokes Equation

Without the control ($b = 0$), using Fourier series for the 2D NS equation (2.1),

$$\Omega = \sum_{k \in \mathbb{Z}^2 / \{0\}} \omega_k e^{i(k_1 x_1 + \alpha k_2 x_2)}, \quad f = \sum_{k \in \mathbb{Z}^2 / \{0\}} F_k e^{i(k_1 x_1 + \alpha k_2 x_2)},$$

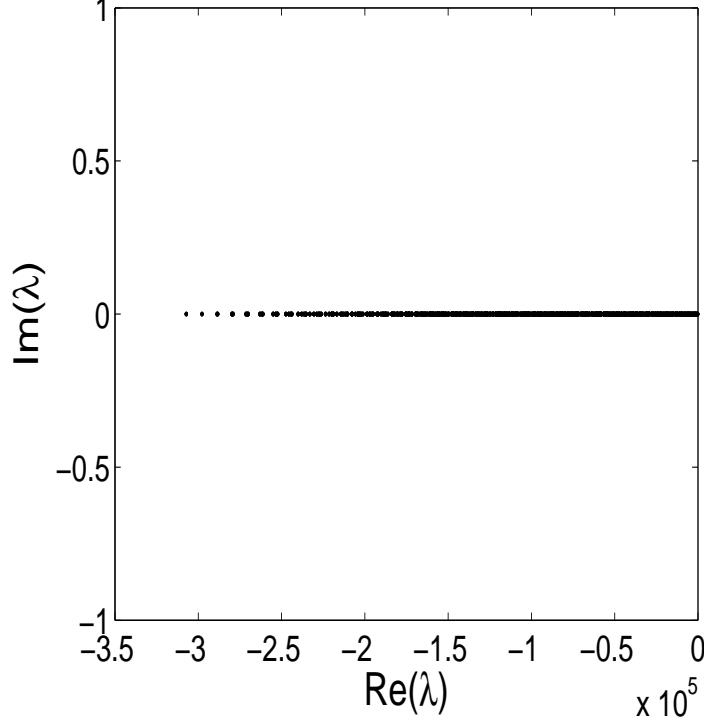


FIGURE 13. The spectrum of the linear NS operator (2.6) where $\epsilon = 150$, $m = 1$ and $\gamma = 0.5$.

where $\omega_{-k} = \overline{\omega_k}$ and $F_{-k} = \overline{F_k}$ (in fact, we always work in the subspace where all the ω_k 's and F_k 's are real-valued), one gets the kinetic form of 2D NS

$$\dot{\omega}_k = \sum_{k=m+n} A(m, n) \omega_m \omega_n + \epsilon (-[k_1^2 + (\alpha k_2)^2] \omega_k + F_k) ,$$

where

$$A(m, n) = \frac{\alpha}{2} \left[\frac{1}{n_1^2 + (\alpha n_2)^2} - \frac{1}{m_1^2 + (\alpha m_2)^2} \right] \begin{vmatrix} m_1 & n_1 \\ m_2 & n_2 \end{vmatrix} .$$

For the numerical simulation of chaos, we continue the study on the Galerkin truncation: $\{|k_1| \leq 2, |k_2| \leq 2\}$. We will use the Melnikov integral (3.1) to test the existence of chaos. We always start from the initial condition (4.1). We choose the external force

$$(5.1) \quad f = a \sin t \cos(x_1 + \alpha x_2) .$$

Then the Melnikov integral (3.1) has the expression

$$(5.2) \quad M_0 = M_1 + a \sqrt{M_2^2 + M_3^2} \sin(t_0 + \theta) ,$$

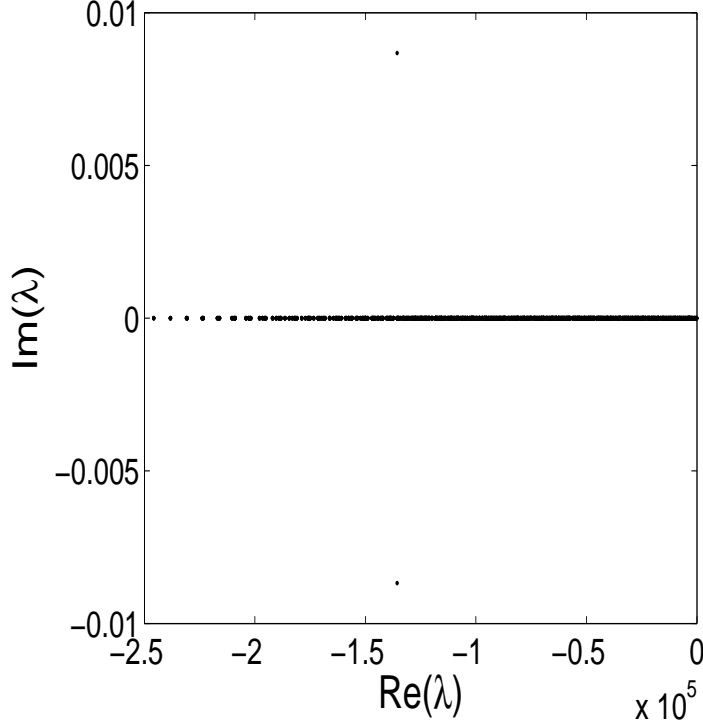


FIGURE 14. The spectrum of the linear NS operator (2.6) where $\epsilon = 120$, $m = 1$ and $\gamma = 0.5$.

where

$$\sin \theta = \frac{M_3}{\sqrt{M_2^2 + M_3^2}}, \quad \cos \theta = \frac{M_2}{\sqrt{M_2^2 + M_3^2}},$$

$$M_1 = \frac{\alpha}{4\pi^2} \int_{-\infty}^{+\infty} \int_0^{2\pi/\alpha} \int_0^{2\pi} (\Omega + \Delta^{-1}\Omega)\Delta\Omega \, dx_1 dx_2 dt,$$

$$M_2 = \frac{\alpha}{4\pi^2} \int_{-\infty}^{+\infty} \int_0^{2\pi/\alpha} \int_0^{2\pi} (\Omega + \Delta^{-1}\Omega) \cos t \cos(x_1 + \alpha x_2) \, dx_1 dx_2 dt,$$

$$M_3 = \frac{\alpha}{4\pi^2} \int_{-\infty}^{+\infty} \int_0^{2\pi/\alpha} \int_0^{2\pi} (\Omega + \Delta^{-1}\Omega) \sin t \cos(x_1 + \alpha x_2) \, dx_1 dx_2 dt,$$

where $\Omega(t)$ is the approximate heteroclinic orbit in Figure 23 with $\Omega(0)$ given by (4.1). The time integral is in fact over the interval $[-11.8, 11.8]$ rather than $(-\infty, \infty)$. Direct numerical computation gives that

$$M_1 = -29.0977, \quad M_2 = -0.06754695, \quad M_3 = 0.$$

Setting $M_0 = 0$ in (5.2), we obtain that

$$\sin(t_0 + \pi) = \frac{430.77741}{a}.$$

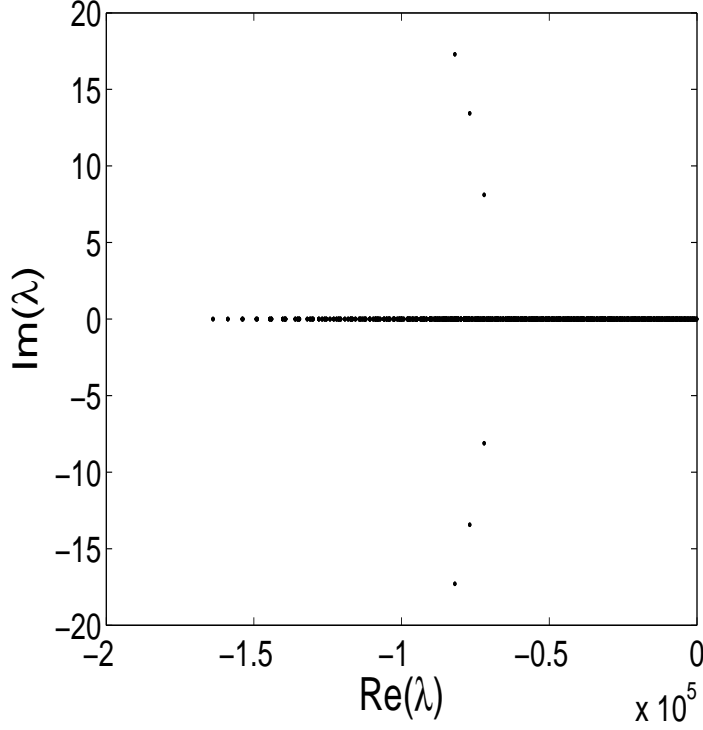


FIGURE 15. The spectrum of the linear NS operator (2.6) where $\epsilon = 80$, $m = 1$ and $\gamma = 0.5$.

Thus, when

$$(5.3) \quad |a| > 430.77741 ,$$

there are solutions to $M_0 = 0$. Next we will test the Melnikov criterion (5.3) and see if it is related to chaos. We define an average Liapunov exponent σ in the following manner: For a large time interval $t \in [0, T]$, let $t_0 = T$ and

$$t_n = T + n2\pi , \quad \text{where } 0 \leq n \leq N , \text{ and } N = 10^3 \text{ or } 2 \times 10^3 .$$

We define

$$\sigma_n = \frac{1}{2\pi} \ln \frac{\|\Delta\omega(t_n + 2\pi)\|}{\|\Delta\omega(t_n)\|} .$$

Then the average Liapunov exponent σ is given by

$$\sigma = \frac{1}{N} \sum_{n=0}^{N-1} \sigma_n .$$

We introduce the Poincaré return map on the section given by $\omega(1, 0) = 0$ and we only record one direction intersection (from $\omega(1, 0)$ positive to negative). For a large time interval $t \in [0, T]$, we only record the last 1000 intersections and we use \bullet to denote the intersections with the two heteroclinic cycles. All the numerical simulations start from the initial condition (4.1). The average Liapunov exponent computed here depends on the time interval, the ensemble of average, and computer

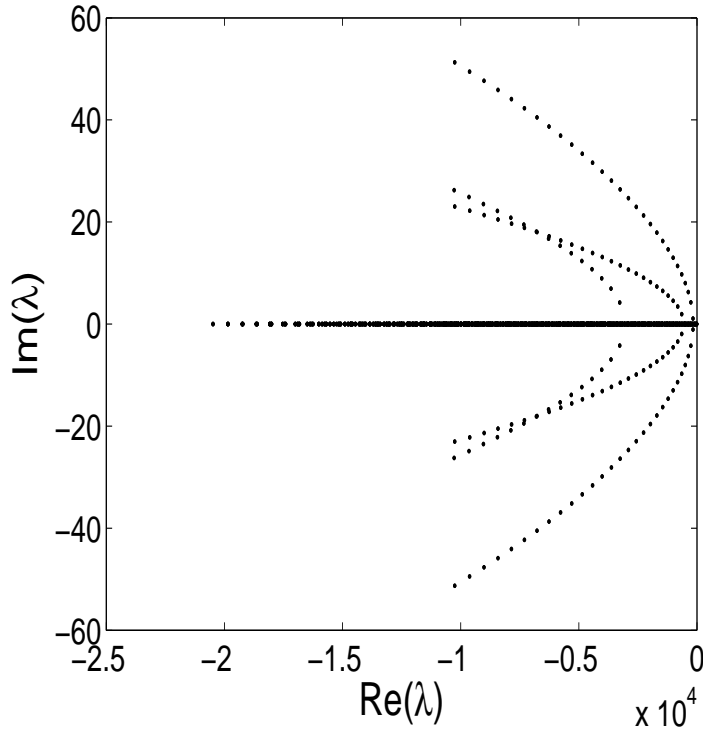


FIGURE 16. The spectrum of the linear NS operator (2.6) where $\epsilon = 10$, $m = 1$ and $\gamma = 0.5$.

accuracy. It only makes sense when it is compared in the same setting. When $\epsilon = 0$, there is no dissipation and no forcing. For a large time interval $t \in [0, T]$, the average Liapunov exponent σ is as follows:

$$\begin{array}{cccc} T = 4 \times 10^4 \pi & T = 8 \times 10^4 \pi & T = 12 \times 10^4 \pi & T = 80 \times 10^4 \pi , \\ \sigma = 0.042 & \sigma = 0.0344 & \sigma = 0.044 & \sigma = 0.0848 . \end{array}$$

Figures 24-25 are the corresponding Poincaré return map plots. The dynamics is chaotic. It seems that the life time of the chaos is infinite (i.e. non-transient chaos).

When $\epsilon > 0$, we find that in all the cases that we tested, the dynamics is always a transient chaos. The Melnikov criterion is only some sort of necessary condition for the existence of heteroclinic chaos [16]. When the Melnikov integral is zero, it gives an indication of a re-intersection of the broken heteroclinic orbit with certain large dimensional center-stable manifold [16]. We believe that such a re-intersection will be reflected by the Liapunov exponent as inducing transient chaos. When $\epsilon = 10^{-5}$, $a \in [0, 1208]$, and $T = 4 \times 10^4 \pi$, we find that

$$\sigma \sim 10^{-4} .$$

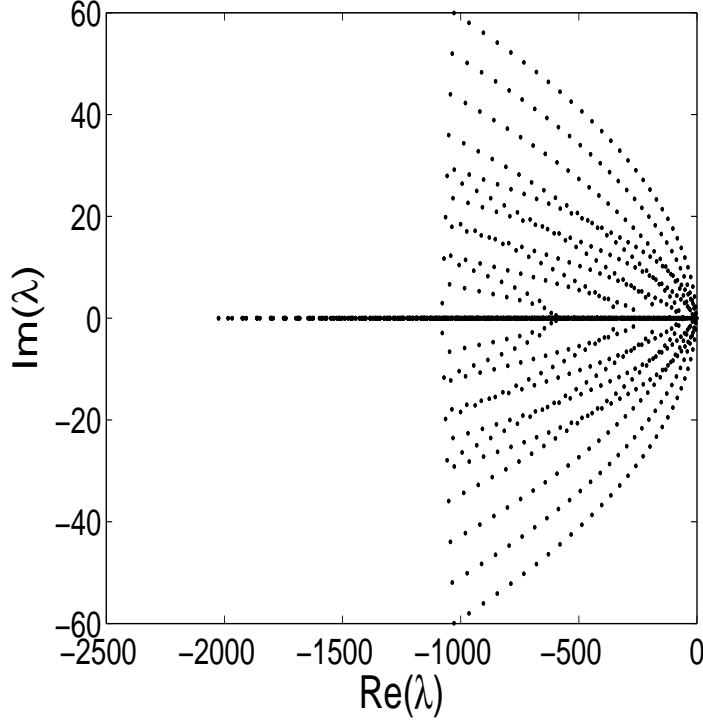


FIGURE 17. The spectrum of the linear NS operator (2.6) where $\epsilon = 1$, $m = 1$ and $\gamma = 0.5$.

For instances,

$$(5.4) \quad \begin{array}{ccccc} a = 400 & a = 430 & a = 440 & a = 650 & a = 850 , \\ \sigma = 4.9 \times 10^{-4} & \sigma = 2.6 \times 10^{-4} & \sigma = 5.3 \times 10^{-4} & \sigma = 5.9 \times 10^{-4} & \sigma = 1.0 \times 10^{-4} . \end{array}$$

But we discover a sharp jump of σ near $a = 1208$ as shown below:

$$(5.5) \quad \begin{array}{cccccc} & T = 2 \times 10^4 \pi & T = 4 \times 10^4 \pi & T = 8 \times 10^4 \pi & T = 8 \times 10^5 \pi , \\ a = 1208 & \sigma = 3.6 \times 10^{-4} & \sigma = 3.9 \times 10^{-4} & \sigma = 4.1 \times 10^{-4} & \sigma = 0 , \\ a = 1208.2 & \sigma = 6.1 \times 10^{-2} & \sigma = 6.1 \times 10^{-2} & \sigma = 2.5 \times 10^{-2} & \sigma = 0 . \end{array}$$

For $T = 4 \times 10^4 \pi$, the corresponding Poincaré return map plots are shown in Figures 26-27. When $T = 80 \times 10^4 \pi$, the chaos for the $a = 1208.2$ case also disappears. When $a > 1208.2$, σ can still be $\sim 10^{-4}$. But we did not observe any sharp jump of σ . We believe that the sharp jump of σ near $a = 1208$ is due to the generation of new transient heteroclinic chaos. Our Melnikov integral calculation predicts when $|a| > 430.77741$, the broken heteroclinic orbit re-intersects with certain center-stable manifold. This does not mean that new heteroclinic orbit is automatically generated. Perhaps near $a = 1208$, new heteroclinic cycle is generated and leads to transient heteroclinic chaos. Since our analysis cannot access such information in the phase space, our comments here are purely speculations.

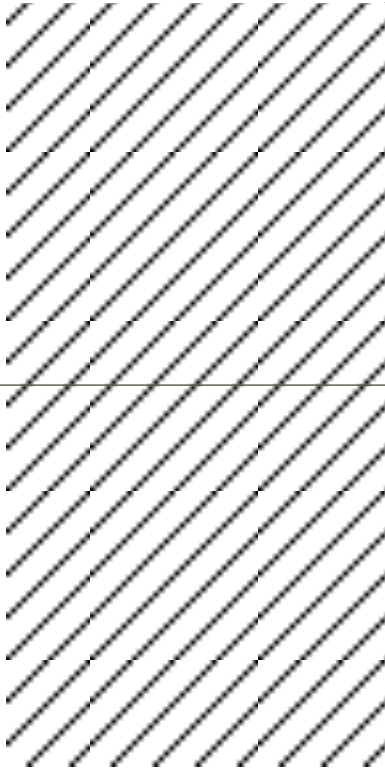


FIGURE 18. The limiting picture of the spectrum of the linear NS operator (2.6) as $\epsilon \rightarrow 0$, where $m = 1$ and $\gamma = 0.5$.

Remark 5.1. We have also conducted numerical experiments on Galerkin truncations by keeping more modes: $\{|k_1| \leq 4, |k_2| \leq 4\}$ and $\{|k_1| \leq 8, |k_2| \leq 8\}$. We found that when $\epsilon = 0$, the strength of chaos increases as the modes are increased: For $T = 8 \times 10^3\pi$,

$$\begin{array}{ccc} |k_1|, |k_2| \leq 2 & |k_1|, |k_2| \leq 4 & |k_1|, |k_2| \leq 8, \\ \sigma = 4.7 \times 10^{-2} & \sigma = 1.3 \times 10^{-1} & \sigma = 1.7 \times 10^{-1}. \end{array}$$

Nevertheless, this does not hint that the dynamics of 2D Euler equation is chaotic since all Galerkin truncations are perturbations of the 2D Euler equation. In fact, higher single Fourier modes (as fixed points) have more eigenvalues with positive real parts.

When $\epsilon > 0$, the strength of chaos decreases as the modes are increased. Higher modes have more dissipations. Also all the chaos are transient. After enough time ($\sim 2 \times 10^4\pi$), the $\epsilon = 0$ chaos is almost smeared away by dissipation, we believe that at this stage the re-intersected heteroclinic orbits play a role and can enhance the transient chaos. It is this stage where the Melnikov calculation is effective.

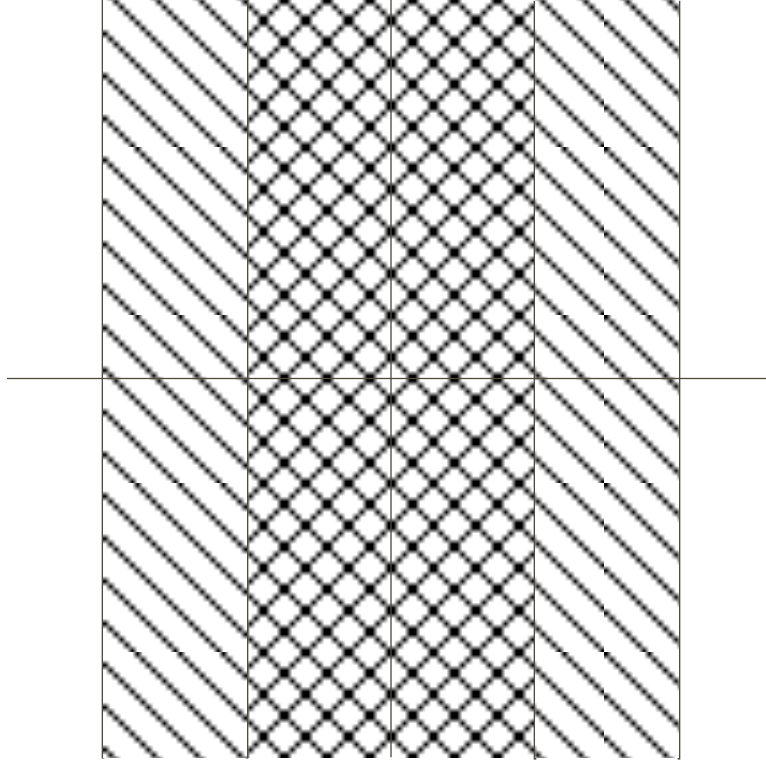


FIGURE 19. The spectrum of the linear Euler operator (2.6) where $\epsilon = 0$, $m = 1$ and $\gamma = 0.5$.

6. Melnikov Integral and Control of Chaos in 2D Navier-Stokes Equation

Now we turn on the control ($b \neq 0$). we continue the study on the Galerkin truncation: $\{|k_1| \leq 2, |k_2| \leq 2\}$. We choose $\tilde{\delta}(x)$ as follows

$$(6.1) \quad \tilde{\delta}(x) = \sum_k e^{i(k_1 x_1 + \alpha k_2 x_2)} .$$

Then the Melnikov integral M in (3.1) is given by

$$(6.2) \quad M = M_0 + bM_c ,$$

where M_0 is given by (5.2) and

$$M_c = \frac{\alpha}{4\pi^2} \int_{-\infty}^{+\infty} \int_0^{2\pi/\alpha} \int_0^{2\pi} (\Omega + \Delta^{-1}\Omega)\tilde{\delta}(x) dx_1 dx_2 dt ,$$

evaluated along the approximate heteroclinic orbit in Figure 23. We find that

$$M_c = -18.6884 .$$

Thus

$$M = -29.0977 - 18.6884 b + 0.06754695 a \sin(t_0 + \pi) .$$

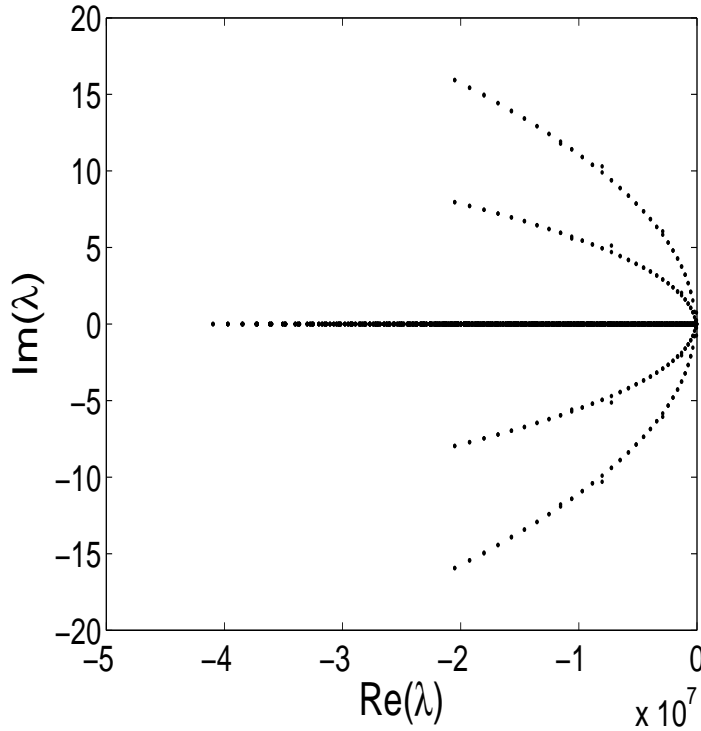


FIGURE 20. The spectrum of the linear NS operator (2.6) where $\epsilon = 20000$, $m = 2$ and $\gamma = 0.5$.

When

$$b = -1.557,$$

the Melnikov integral M has roots for any $a \neq 0$.

All the numerical simulations start from the initial condition (4.1). When $\epsilon = 10^{-5}$, $b = -1.557$, and $T = 10^4\pi$, we find that:

$a = 1$ $\sigma = 7.1 \times 10^{-4}$	$a = 10$ $\sigma = 8.8 \times 10^{-4}$	$a = 200$ $\sigma = 9.3 \times 10^{-4}$	$a = 400$ $\sigma = 9.0 \times 10^{-4}$	$a = 800$, $\sigma = 6.6 \times 10^{-4}$.
$a = 1000$ $\sigma = 8.6 \times 10^{-4}$	$a = 1208$ $\sigma = 8.1 \times 10^{-4}$	$a = 1208.2$ $\sigma = 8.4 \times 10^{-4}$	$a = 1500$ $\sigma = 8.6 \times 10^{-4}$	$a = 3000$, $\sigma = 7.7 \times 10^{-4}$.

In comparison with (5.4), the values of the Liapunov exponents under the control are doubled. Thus the control seems enhancing chaos but not dramatically. We did not observe the sharp jump of the values of σ around $a = 1208$ as in the $b = 0$ case (5.5). Here the control theory is not as rigorous as that of sine-Gordon system in Appendix A. But we believe that the Melnikov integral can play a significant role in the control of chaos in NS equation. After all, the chaos in NS is generated by instabilities characterized by unstable eigenvalues. And these unstable eigenvalues persist for Euler equation as shown in a previous section. For Euler equation, these unstable eigenvalues characterize hyperbolic structures which are very likely of heteroclinics type due to infinitely many constants of motion. Thus Melnikov

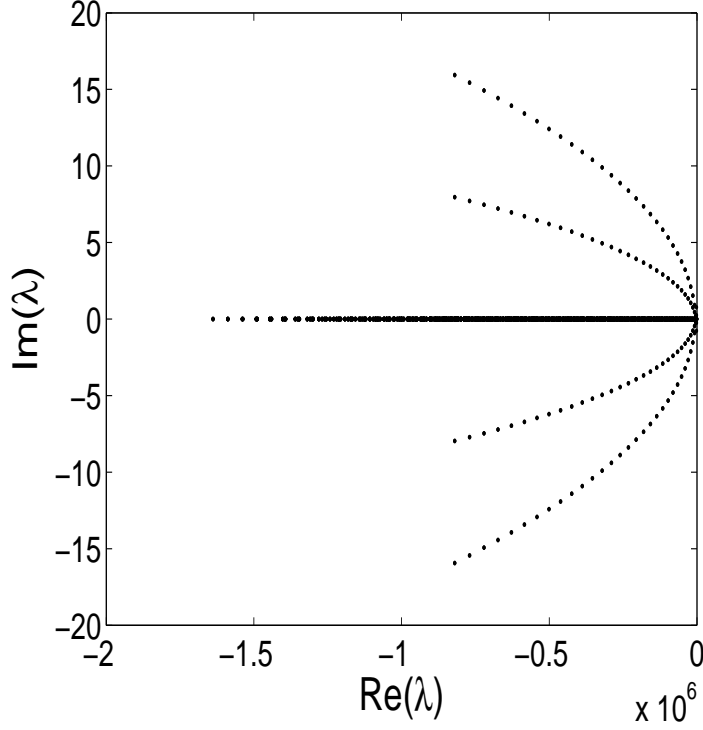


FIGURE 21. The spectrum of the linear NS operator (2.6) where $\epsilon = 800$, $m = 2$ and $\gamma = 0.5$.

integrals supported upon these hyperbolic structures should play an important role in predicting and controlling chaos.

7. Zero Viscosity Limit of the Spectrum of 3D Linear Navier-Stokes Operator

We will study the following form of 3D Navier-Stokes equation with a control,

$$(7.1) \quad \partial_t \Omega + (u \cdot \nabla) \Omega - (\Omega \cdot \nabla) u = \epsilon [\Delta \Omega + f(t, x) + b \tilde{\delta}(x)] ,$$

where $u = (u_1, u_2, u_3)$ is the velocity, $\Omega = (\Omega_1, \Omega_2, \Omega_3)$ is the vorticity, $\nabla = (\partial_{x_1}, \partial_{x_2}, \partial_{x_3})$, $\Omega = \nabla \times u$, $\nabla \cdot u = 0$, $\epsilon = 1/\text{Re}$ is the inverse of the Reynolds number, Δ is the 3D Laplacian, and $f(t, x) = (f_1(t, x), f_2(t, x), f_3(t, x))$ is the external force, $b \tilde{\delta}(x)$ is the spatially localized control, and b is the control parameter. We also pose periodic boundary condition of period $(2\pi/\alpha, 2\pi/\beta, 2\pi)$, i.e. the 3D NS is defined on the 3-torus \mathbb{T}^3 . We require that u , Ω , f and $\tilde{\delta}$ all have mean zero. In this case, u can be uniquely determined from Ω by Fourier transform:

$$\begin{aligned} U_1(k) &= i|k|^{-2}[k_2\omega_3(k) - k_3\omega_2(k)] , \\ U_2(k) &= i|k|^{-2}[k_3\omega_1(k) - k_1\omega_3(k)] , \\ U_3(k) &= i|k|^{-2}[k_1\omega_2(k) - k_2\omega_1(k)] , \end{aligned}$$

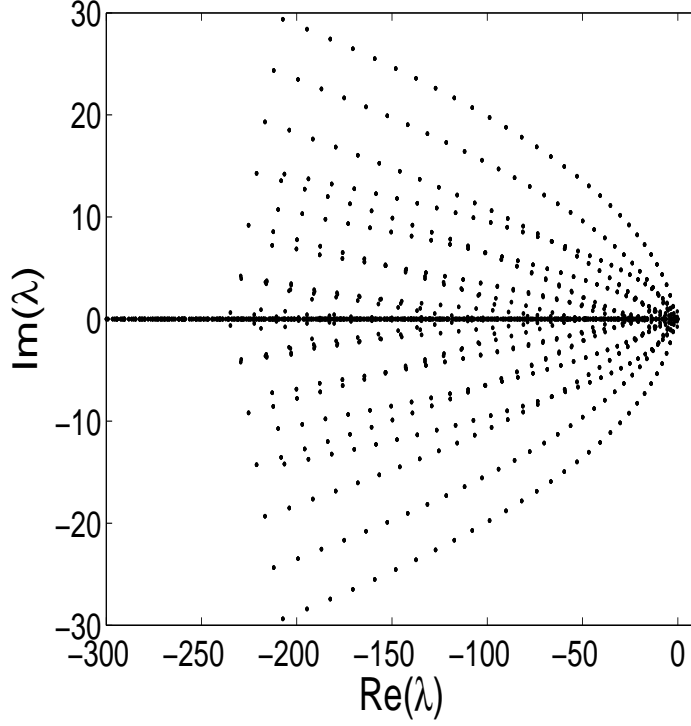


FIGURE 22. The spectrum of the linear NS operator (2.6) where $\epsilon = 0.2$, $m = 2$ and $\gamma = 0.5$.

which can be rewritten in the compact form

$$U_\ell(k) = i|k|^{-2}\varepsilon_{\ell mn}k_m\omega_n(k) ,$$

where $\varepsilon_{\ell mn}$ is the permutation symbol ($\ell, m, n = 1, 2, 3$),

$$k = (k_1, k_2, k_3) = (\alpha\kappa_1, \beta\kappa_2, \kappa_3) , \quad \kappa = (\kappa_1, \kappa_2, \kappa_3) ,$$

$$u_\ell(x) = \sum_{\kappa \in \mathbb{Z}^3 / \{0\}} U_\ell(k)e^{ik \cdot x} , \quad \Omega_\ell(x) = \sum_{\kappa \in \mathbb{Z}^3 / \{0\}} \omega_\ell(k)e^{ik \cdot x} .$$

Using these Fourier transforms together with

$$f_\ell(x) = \sum_{\kappa \in \mathbb{Z}^3 / \{0\}} F_\ell(k)e^{ik \cdot x} , \quad \tilde{\delta}_\ell(x) = \sum_{\kappa \in \mathbb{Z}^3 / \{0\}} \Delta_\ell(k)e^{ik \cdot x} ,$$

we can rewrite the 3D NS (7.1) into the kinetic form

$$\begin{aligned} & \partial_t \omega_\ell(k) + k_s \sum_{\tilde{k}=\hat{k}+\hat{k}} |\tilde{k}|^{-2} \tilde{k}_m \omega_n(\tilde{k}) [\varepsilon_{\ell mn} \omega_s(\hat{k}) - \varepsilon_{smn} \omega_\ell(\hat{k})] \\ (7.2) \quad & = \epsilon [-|k|^2 \omega_\ell(k) + F_\ell(k) + b \Delta_\ell(k)] . \end{aligned}$$

A popular example of fixed points of the 3D NS (7.1) is the so-called ABC flow [2]

$$(7.3) \quad u_1 = A \sin x_3 + C \cos x_2, \quad u_2 = B \sin x_1 + A \cos x_3, \quad u_3 = C \sin x_2 + B \cos x_1,$$

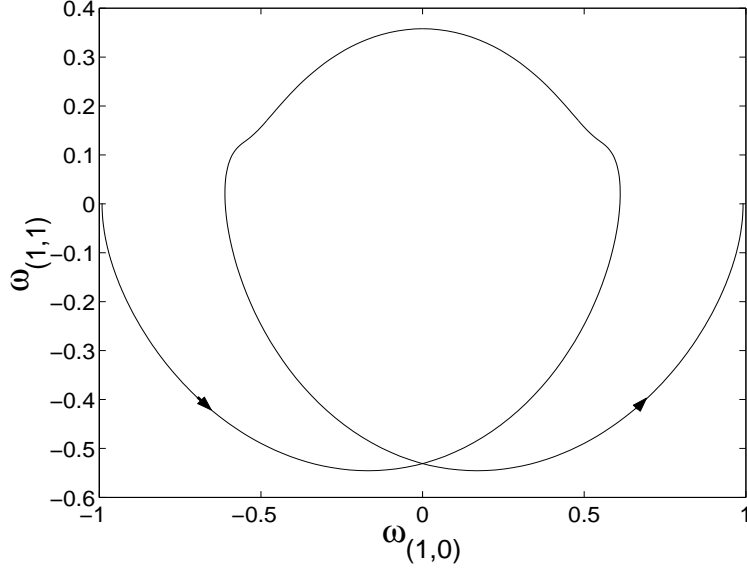


FIGURE 23. The approximate heteroclinic orbit projected onto the $(\omega_{(1,0)}, \omega_{(1,1)})$ -plane in the case of the $\{|k_1| \leq 2, |k_2| \leq 2\}$ Galerkin truncation of the 2D Euler equation.

where $\alpha = \beta = 1$ and $\Omega = u = f$ and $b = 0$. The popularity comes from the fact that the Lagrangian fluid particle flow generated by the vector field (7.3) can still be chaotic [2]. On the other hand, in Appendix B, we prove that the Lagrangian flow generated by any solution to the 2D Euler equation is always integrable.

7.1. A 3D Shear Fixed Point. Below we will study the simplest fixed point – the 3D shear flow (which is also a special case of the ABC flow (7.3) where $A = 2$ and $B = C = 0$):

$$(7.4) \quad \Omega_1 = 2 \sin x_3, \quad \Omega_2 = 2 \cos x_3, \quad \Omega_3 = 0.$$

Let $p = (0, 0, 1)$, the Fourier transform ω^* of the fixed point is given by:

$$\omega_1^*(p) = -i, \quad \omega_2^*(p) = 1, \quad \omega_1^*(-p) = i, \quad \omega_2^*(-p) = 1, \quad \omega_3^*(p) = \omega_3^*(-p) = 0,$$

and $\omega_\ell^*(k) = 0, \forall k \neq p$ or $-p$. We choose $\alpha = 0.7$ and $\beta = 1.3$ hoping that the fixed point ω^* has only one unstable eigenvalue. The spectral equations of the 3D linear NS operator at the fixed point ω^* are given by

$$\begin{aligned} & [(k_1 + ik_2) - ik_2|k - p|^{-2}] \omega_1(k - p) \\ & + [i|k - p|^{-2} k_1 + i|k - p|^{-2} (k_1 + ik_2)(k_3 - 1)] \omega_2(k - p) \\ & + [-1 - ik_2(k_1 + ik_2)|k - p|^{-2}] \omega_3(k - p) + \epsilon|k|^2 \omega_1(k) \\ & + [-(k_1 - ik_2) - ik_2|k + p|^{-2}] \omega_1(k + p) \\ & + [i|k + p|^{-2} k_1 - i|k + p|^{-2} (k_1 - ik_2)(k_3 + 1)] \omega_2(k + p) \\ & + [-1 + ik_2(k_1 - ik_2)|k + p|^{-2}] \omega_3(k + p) = -\lambda \omega_1(k), \end{aligned}$$

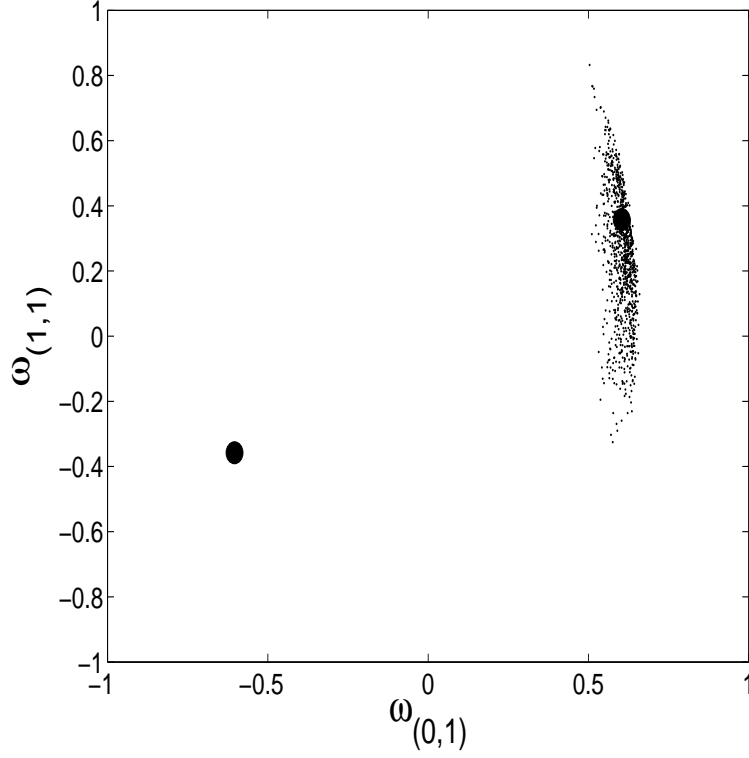


FIGURE 24. The Poincaré return map plot projected onto the plane $(\omega_{(0,1)}, \omega_{(1,1)})$ -plane, in the case of the $\{|k_1| \leq 2, |k_2| \leq 2\}$ Galerkin truncation of the 2D Euler equation (i.e. $\epsilon = 0$), where $t \in [0, T]$, $T = 4 \times 10^4 \pi$, only the last 1000 intersections are recorded.

$$\begin{aligned}
& [k_2|k-p|^{-2} - i(k_3-1)(k_1+ik_2)|k-p|^{-2}]\omega_1(k-p) \\
& + [(k_1+ik_2) - k_1|k-p|^{-2}]\omega_2(k-p) \\
& + [-i + ik_1(k_1+ik_2)|k-p|^{-2}]\omega_3(k-p) + \epsilon|k|^2\omega_2(k) \\
& + [-k_2|k+p|^{-2} + i(k_3+1)(k_1-ik_2)|k+p|^{-2}]\omega_1(k+p) \\
& + [-(k_1-ik_2) + k_1|k+p|^{-2}]\omega_2(k+p) \\
& + [i - ik_1(k_1-ik_2)|k+p|^{-2}]\omega_3(k+p) = -\lambda\omega_2(k) ,
\end{aligned}$$

$$\begin{aligned}
& [ik_2(k_1+ik_2)|k-p|^{-2}]\omega_1(k-p) + [-ik_1(k_1+ik_2)|k-p|^{-2}]\omega_2(k-p) \\
& + [k_1+ik_2]\omega_3(k-p) + \epsilon|k|^2\omega_3(k) + [-ik_2(k_1-ik_2)|k+p|^{-2}]\omega_1(k+p) \\
& + [ik_1(k_1-ik_2)|k+p|^{-2}]\omega_2(k+p) + [-(k_1-ik_2)]\omega_3(k+p) = -\lambda\omega_3(k) .
\end{aligned}$$

Thus the 3D linear NS operator also decouples according to the lines $\hat{k} + jp$ ($j \in \mathbb{Z}$). Next we study the zero viscosity limit of the spectrum of this 3D linear NS operator. When $\hat{k} = (\alpha, 0, 0)$, we have tested the truncation of the line $\hat{k} + jp$ up to $|j| \leq 400$. The deformation pattern stays the same. Below we present the case $|j| \leq 100$ for which the pictures are more clear. Figure 28 shows the case $\epsilon = 2.0$ where all

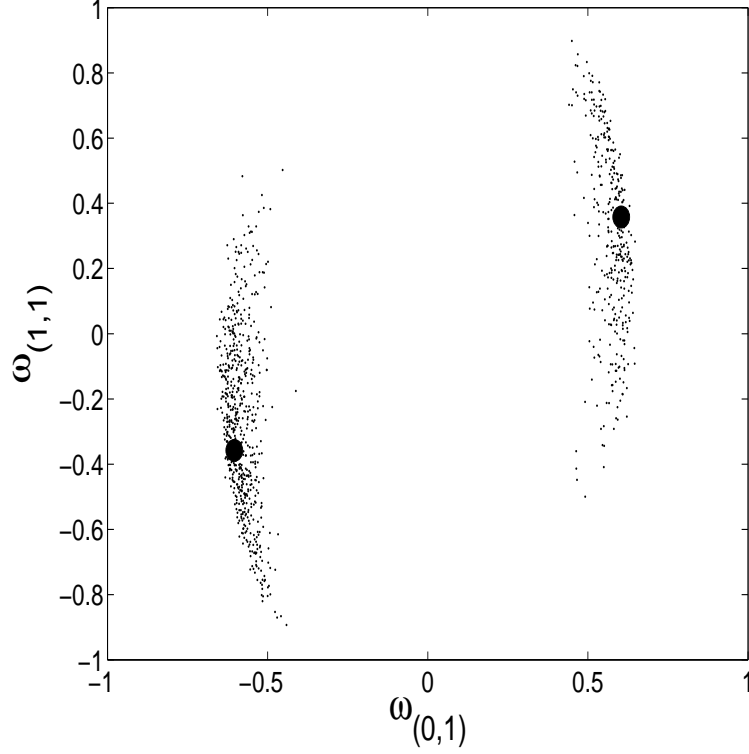


FIGURE 25. The same as Figure 24, except $T = 80 \times 10^4 \pi$.

the eigenvalues are negative. Figure 29 shows the case $\epsilon = 1.8$ where a pair of eigenvalues jumps off the real axis. When $\epsilon \leq 0.66$, a unique positive eigenvalue appears. Figure 28 shows the case $\epsilon = 0.0007$ where a bubble has developed. As $\epsilon \rightarrow 0^+$, the limiting picture is the same with Figure 7. When $\epsilon = 0$, The spectrum picture is the same with Figure 8. All other decoupled systems have the same bifurcation patterns but without the pair of persistent eigenvalues. For the entire spectrum of the 3D linear NS operator, the limiting picture is the same with Figure 11 as $\epsilon \rightarrow 0^+$; and the spectrum is the same with Figure 12 when setting $\epsilon = 0$ [28]. It seems that the Unstable Disk Theorem [10] of the 2D linear Euler case is still valid: $|\hat{k} + jp| < |p|$ for some j , implies that there is an eigenvalue of positive real part; while $|\hat{k} + jp| > |p|$ for all j , implies that there is no eigenvalue of positive real part.

7.2. The ABC Fixed Point. In this case, the periodic domain is the cube, i.e. $\alpha = \beta = 1$. The ABC flow is given specifically by

$$\Omega_1^* = A \sin mx_3 + C \cos mx_2, \quad \Omega_2^* = B \sin mx_1 + A \cos mx_3, \quad \Omega_3^* = C \sin mx_2 + B \cos mx_1,$$

where m is a positive integer, and (A, B, C) are real parameters. In terms of Fourier modes: Let $p = (m, 0, 0)$, $q = (0, m, 0)$, and $r = (0, 0, m)$, then the ABC flow is

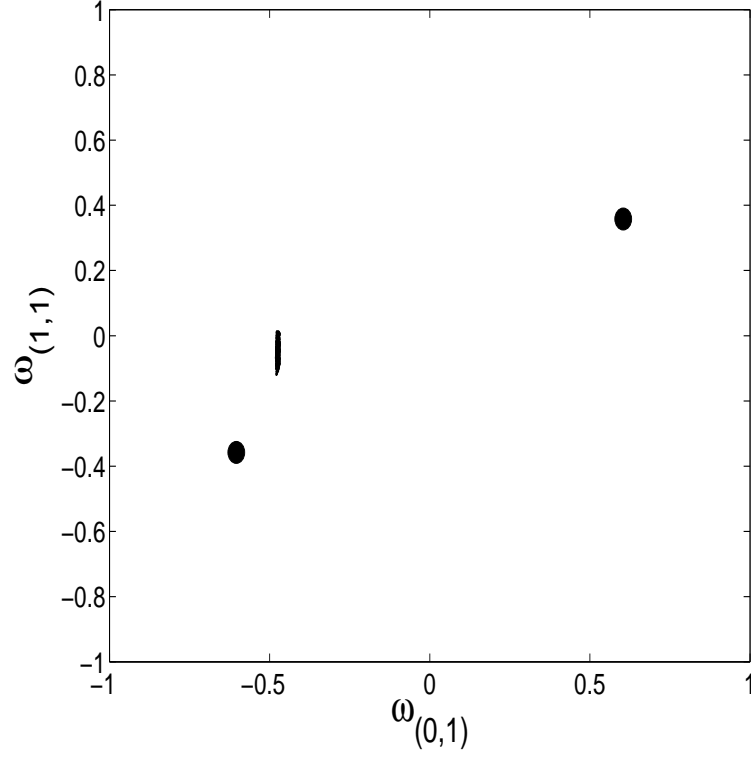


FIGURE 26. The same as Figure 24, except $\epsilon = 10^{-5}$, $a = 1208$, and $T = 2 \times 10^4 \pi$.

given by

$$\begin{aligned}
 \omega_1^*(q) &= \frac{1}{2}C, \quad \omega_1^*(-q) = \frac{1}{2}C, \\
 \omega_1^*(r) &= \frac{1}{2i}A, \quad \omega_1^*(-r) = -\frac{1}{2i}A, \\
 \omega_2^*(p) &= \frac{1}{2i}B, \quad \omega_2^*(-p) = -\frac{1}{2i}B, \\
 \omega_2^*(r) &= \frac{1}{2}A, \quad \omega_2^*(-r) = \frac{1}{2}A, \\
 \omega_3^*(p) &= \frac{1}{2}B, \quad \omega_3^*(-p) = \frac{1}{2}B, \\
 \omega_3^*(q) &= \frac{1}{2i}C, \quad \omega_3^*(-q) = -\frac{1}{2i}C.
 \end{aligned}$$

The spectral equation for the linear 3D NS operator at the ABC flow is then given by

$$\begin{aligned}
 \lambda \omega_\ell(k) &= -\epsilon |k|^2 \omega_\ell(k) - k_s \sum_{\tilde{k}=\hat{k}+\check{k}} \left[|\tilde{k}|^{-2} \tilde{k}_m \omega_n^*(\tilde{k}) [\varepsilon_{\ell mn} \omega_s(\hat{k}) - \varepsilon_{smn} \omega_\ell(\hat{k})] \right. \\
 &\quad \left. + |\check{k}|^{-2} \check{k}_m \omega_n(\check{k}) [\varepsilon_{\ell mn} \omega_s^*(\hat{k}) - \varepsilon_{smn} \omega_\ell^*(\hat{k})] \right].
 \end{aligned}$$

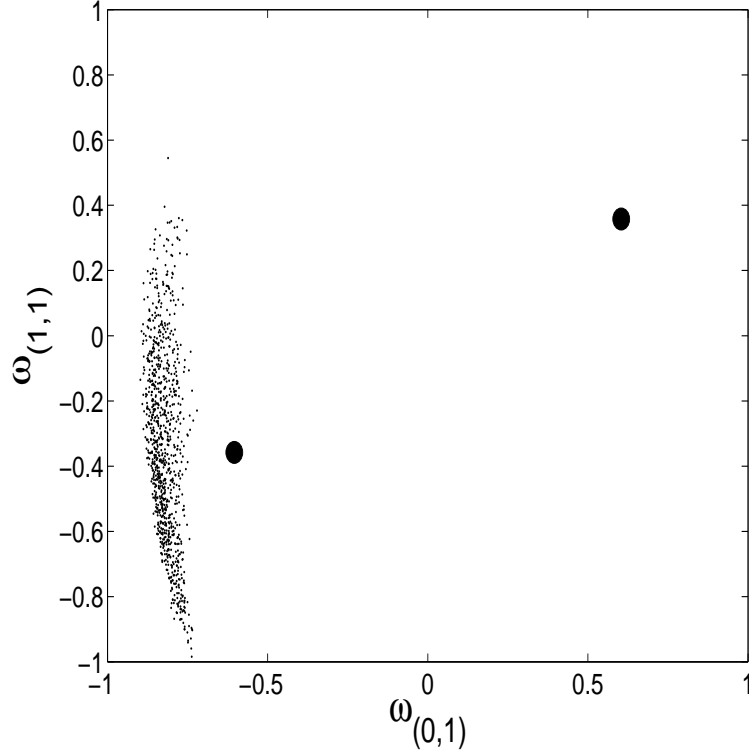


FIGURE 27. The same as Figure 24, except $\epsilon = 10^{-5}$, $a = 1208.2$, and $T = 2 \times 10^4\pi$.

Calculating the eigenvalues of the Galerkin truncations of this system becomes challenging. Beyond the size $\{|k_n| \leq 6, n = 1, 2, 3\}$, the computing time is too long. Below we present some pictures for the Galerkin truncation $\{|k_n| \leq 4, n = 1, 2, 3\}$. We choose $m = 1$, $A = 1.2$, $B = 0.7$ and $C = 0.9$. When $\epsilon = 20000$, all the eigenvalues are negative as shown in Figure 31. As ϵ is decreased, eigenvalues start to jump off the real axis and form vertical lines as shown in Figure 32 when $\epsilon = 10$, in contrast to the parabolas in the cases of cat's eye and 3D shear. When ϵ is decreased to $\epsilon = 0.1$, many eigenvalues move to the right half plane, i.e. there are many unstable eigenvalues as shown in Figure 33. Notice that for the full linear NS operator, there should be an infinite tail of negative eigenvalues to the left. When $\epsilon = 0$, the eigenvalues of the Galerkin truncation of linear NS are symmetric with respect to the real and imaginary axes as shown in Figure 34. When $\epsilon = 0$, the full linear Euler operator at the ABC flow has a continuous spectrum similar to that at the cat's eye [28]. That is, the continuous spectrum of the linear Euler at the ABC flow, in any Sobolev space $H^s(\mathbb{T}^2)$ where s is a non-negative integer, is a vertical band of width $2s\sigma$ symmetric with respect to the imaginary axis $\{\lambda : |\operatorname{Re}(\lambda)| \leq s\sigma\}$ as shown in Figure 19, where $\sigma > 0$ is the largest Liapunov exponent of the vector field given by ABC flow. Thus the width of the vertical band is proportional to the scale s of the Sobolev space $H^s(\mathbb{T}^2)$ [28]. The union of all such bands for all integers $s \geq 0$ is the entire complex plane. The eigenfunctions of the linear NS

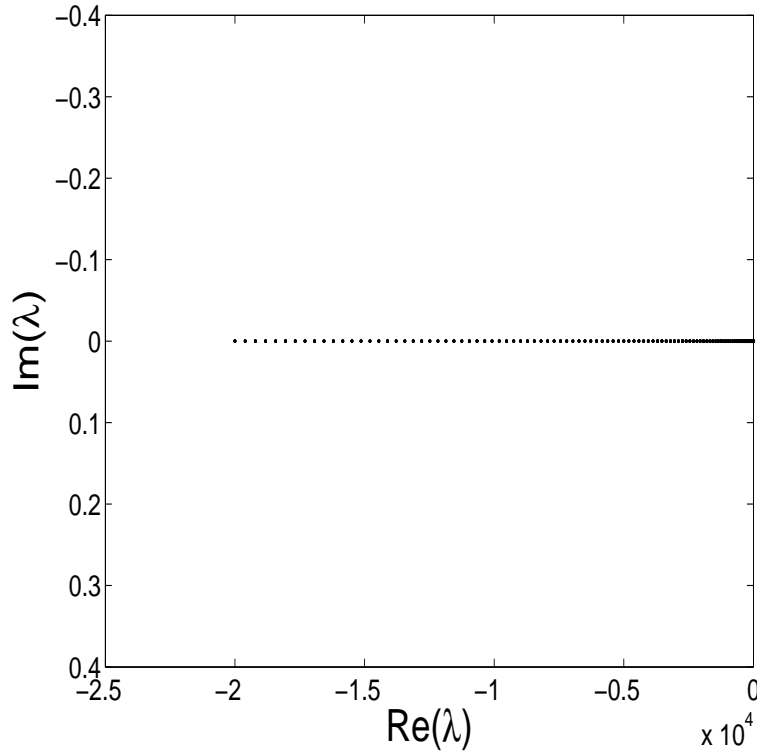


FIGURE 28. The eigenvalues of the line $\hat{k} = (\alpha, 0, 0)$ are all negative when $\epsilon = 2.0$.

at the ABC flow when $\epsilon > 0$ belong to $H^s(\mathbb{T}^2)$ for all integers $s \geq 0$. As ϵ is decreased, the eigenvalues move into the right half plane. The $\epsilon \rightarrow 0^+$ limiting picture of the eigenvalues of the linear NS at the ABC flow is that the eigenvalues are dense on the entire plane, in contrast to the left half plane in the case of cat's eye as shown in Figure 18. That is, all the eigenvalues of the linear NS at the ABC flow condense into the entire plane – “condensation”. Thus the possible instability hinted by the right half band of the continuous spectrum of linear Euler in $H^s(\mathbb{T}^2)$ may be realized by real viscous fluids in this case in contrast to the cat's eye case.

8. Numerical Verification of the Heteroclinics Conjecture for 3D Euler Equations

For 3D Euler equations, one can also pose the heteroclinics conjecture.

- The Heteroclinics Conjecture: There is a heteroclinic orbit of the 3D Euler equations that connects Ω (7.4) and $-\Omega$.

As discussed in the Introduction, the rationality of this conjecture comes from the fact that 3D Euler equations have a Lax pair [23]. Below we will verify this conjecture for the Galerkin truncation: $|\kappa_n| \leq 1$ ($n = 1, 2, 3$) where $k = (\alpha\kappa_1, \beta\kappa_2, k_3)$. Even though this is the smallest Galerkin truncation, the dimension of the resulting system is still very large. For this Galerkin truncation, the fixed point (7.4) is still a fixed point. The linearized Galerkin truncation operator at this fixed point can be

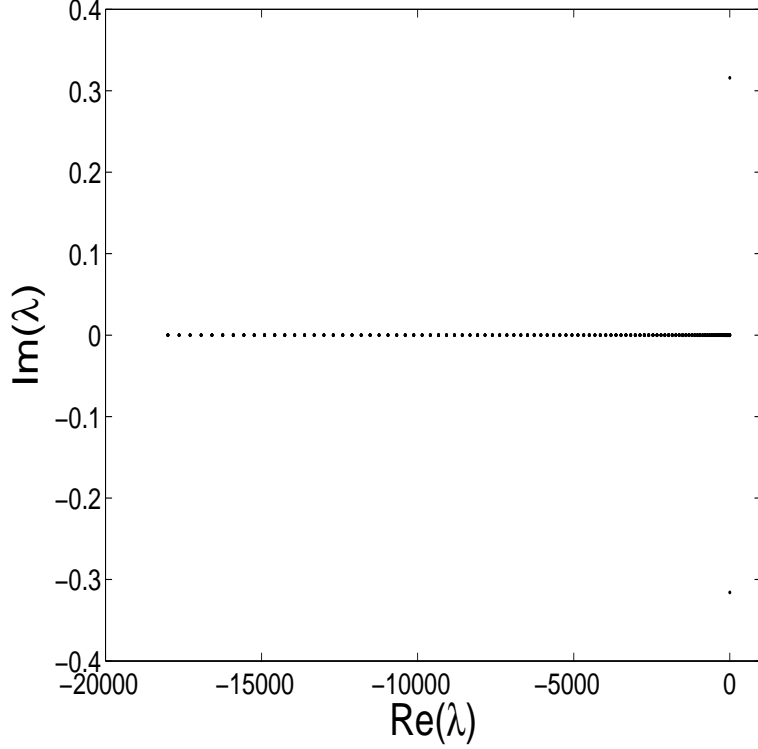


FIGURE 29. A pair of eigenvalues of the line $\hat{k} = (\alpha, 0, 0)$ jumps off the real axis when $\epsilon = 1.8$.

obtained by the corresponding Galerkin truncation the 3D linear Euler operator. In this case, the line segment labeled by $\hat{k} = (\alpha, 0, 0)$ ($\epsilon = 0$) has a positive eigenvalue $\lambda = 0.5792$, and the corresponding eigenvector v is given by:

$$\begin{aligned} \omega_1(1, 0, -1) &= 0.328919 - i 0.246347, & \omega_2(1, 0, -1) &= -0.246347 - i 0.328919, \\ \omega_3(1, 0, -1) &= 0.230243 - i 0.172443, & \omega_1(1, 0, 0) &= 0, \\ \omega_2(1, 0, 0) &= -0.19583 - i 0.26147, \\ \omega_3(1, 0, 0) &= 0.183029 - i 0.137081, & \omega_1(1, 0, 1) &= 0.328919 - i 0.246347, \\ \omega_2(1, 0, 1) &= 0.246347 + i 0.328919, & \omega_3(1, 0, 1) &= -0.230243 + i 0.172443, \end{aligned}$$

and all other $\omega_\ell(k)$'s are zero. Starting from the initial condition

$$(8.1) \quad \omega = \omega^* + 10^{-3}v,$$

where ω^* is the Fourier transform of the fixed point (7.4), the approximate heteroclinic orbit reaches order $\sim 10^{-3}$ neighborhood of $-\omega^*$ during the time interval $[0, 29.33]$. This approximate heteroclinic orbit is the lower branch of the approximate heteroclinic cycle shown in Figure 35. Notice that the approximate heteroclinic orbit here does not have the extra loop as in Figure 23. When more modes are included in the Galerkin truncation, extra loops may be generated.

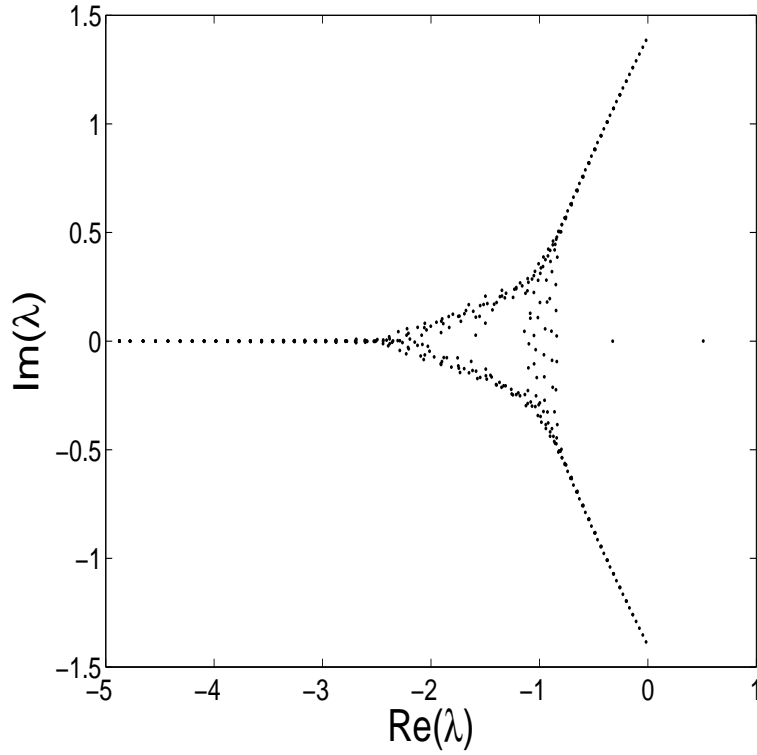


FIGURE 30. A bubble of eigenvalues of the line $\hat{k} = (\alpha, 0, 0)$ has developed when $\epsilon = 0.0007$.

9. Melnikov Integral and Numerical Simulation of Chaos in 3D Navier-Stokes Equation

Setting $\epsilon = 0$ in the 3D NS (7.1), one gets the corresponding 3D Euler equation for which one has the following constants of motion:

$$E = \int_{\mathbb{T}^3} |u|^2 dx, \quad H = \int_{\mathbb{T}^3} u \cdot \Omega dx$$

where E is the kinetic energy and H is the helicity. We will use the constant of motion

$$G = E - H = \int_{\mathbb{T}^3} |u|^2 dx - \int_{\mathbb{T}^3} u \cdot \Omega dx$$

to build a Melnikov integral for the corresponding 3D Navier-Stokes equation (7.1). We will try to make use of the Melnikov integral as a measure of chaos and to conduct a control of chaos, around the 3D shear flow (7.4). The gradient of G in u or Ω is given by

$$\nabla_u G = 2(u - \Omega), \quad \nabla_\Omega G = 2 \operatorname{curl}^{-1}(u - \Omega),$$

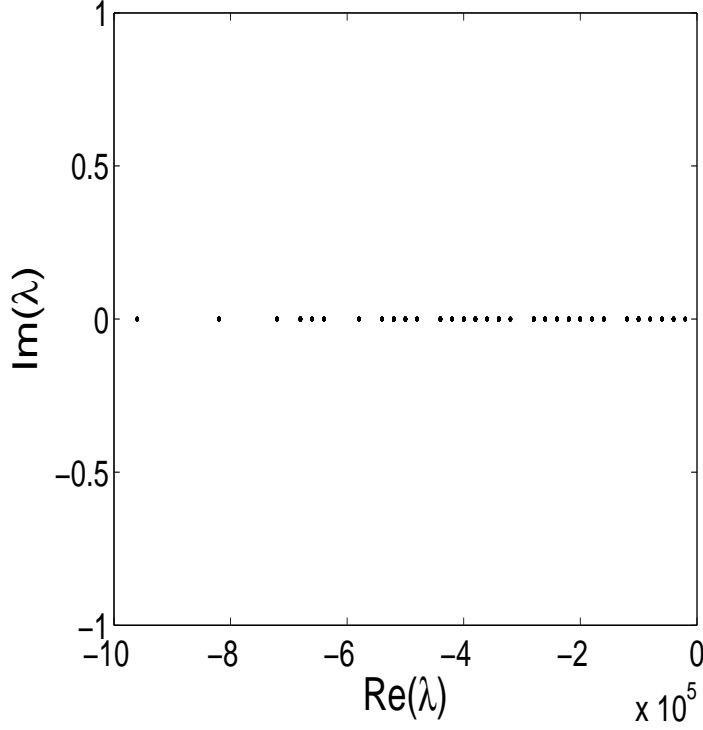


FIGURE 31. The eigenvalues of the (Galerkin truncation of) linear NS at the ABC flow when $\epsilon = 20000$.

where $\text{curl} = \nabla \times \cdot$. The gradient is zero at the 3D shear flow (7.4). We define the Melnikov function for the 3D NS (7.1) as

$$\begin{aligned} M &= \frac{\alpha\beta}{16\pi^3} \int_{-\infty}^{+\infty} \int_{\mathbb{T}^3} \nabla_{\Omega} G[\Delta\Omega + f(t, x) + b\tilde{\delta}(x)] dx dt \\ &= \frac{\alpha\beta}{16\pi^3} \int_{-\infty}^{+\infty} \int_{\mathbb{T}^3} 2 \text{curl}^{-1}(u - \Omega)[\Delta\Omega + f(t, x) + b\tilde{\delta}(x)] dx dt . \end{aligned}$$

Next we conduct numerical simulations on the Galerkin truncation $|\kappa_n| \leq 1$ ($n = 1, 2, 3$). When $\epsilon = 0$, the Liapunov exponent $\sigma = 0$ for all the numerical tests that we run. This indicates that there is no chaos when $\epsilon = 0$. Often the smallest Galerkin truncation is an integrable system [12] [22]. In such a circumstance, the Melnikov integral represents the leading order term of the distance between the broken heteroclinic orbit and the center-stable manifold of the fixed point. But the dimension of the center-stable manifold is large. The zero of the Melnikov integral implies that the unstable manifold in which the broken heteroclinic orbit lives, intersects with the center-stable manifold. Therefore, there is a new heteroclinic orbit which lives in the intersection. Such a heteroclinic orbit does not immediately imply the existence of chaos, even though it may lead to some transient chaos characterized by finite time positive Liapunov exponent (infinite time positive Liapunov exponent is zero). To compute the Melnikov integral, we choose the external force

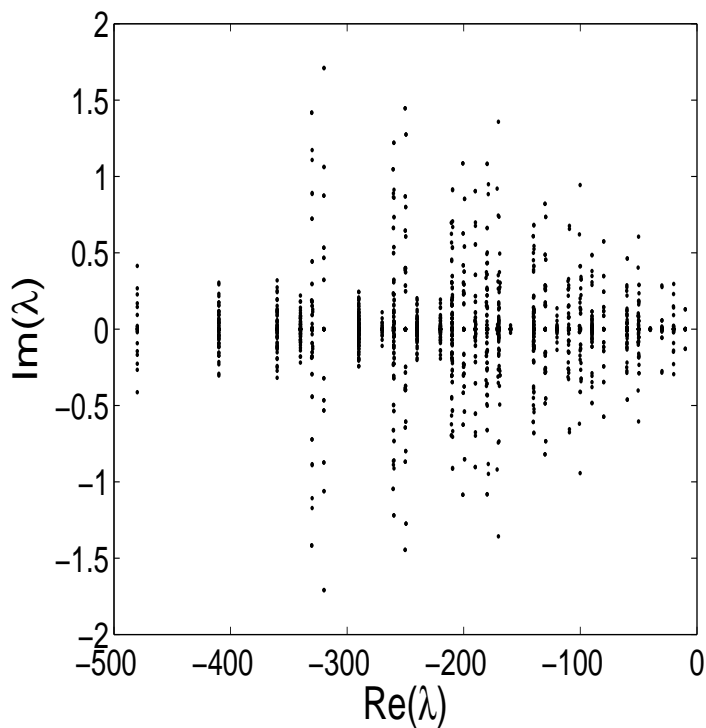


FIGURE 32. The eigenvalues of the (Galerkin truncation of) linear NS at the ABC flow when $\epsilon = 10$.

and control as follows

$$\begin{aligned}
 f_1 &= a \sin t \cos(x_1 + \alpha x_2), & f_2 &= f_3 = 0, \\
 \tilde{\delta}_1(x) &= \sum_{\kappa} e^{ik \cdot x}, & \tilde{\delta}_2 &= \tilde{\delta}_3 = 0,
 \end{aligned}$$

where the sum is over the Galerkin truncation. Then the Melnikov integral has the expression

$$(9.1) \quad M = M_1 + a \sqrt{M_2^2 + M_3^2} \sin(t_0 + \theta) + b M_4,$$

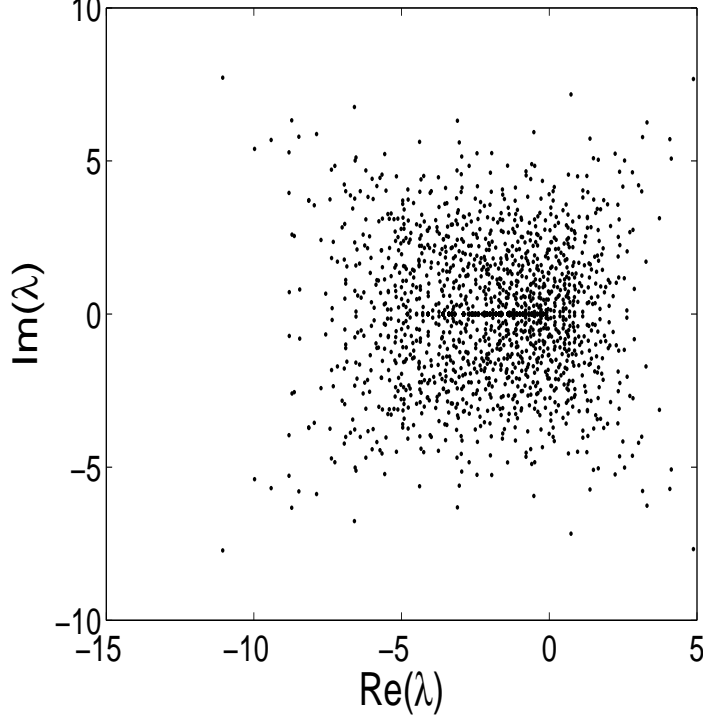


FIGURE 33. The eigenvalues of the (Galerkin truncation of) linear NS at the ABC flow when $\epsilon = 0.1$.

where

$$\sin \theta = \frac{M_3}{\sqrt{M_2^2 + M_3^2}}, \quad \cos \theta = \frac{M_2}{\sqrt{M_2^2 + M_3^2}},$$

$$M_1 = - \int_{-\infty}^{+\infty} \sum_k \operatorname{Re} \left\{ i \varepsilon_{\ell mn} k_m (i|k|^{-2} \varepsilon_{nsr} k_s \omega_r - \omega_n) \overline{\omega_\ell(k)} \right\} dt,$$

$$M_2 = \int_{-\infty}^{+\infty} \cos t \operatorname{Re} \left\{ i|k|^{-2} \varepsilon_{1mn} k_m (i|k|^{-2} \varepsilon_{nsr} k_s \omega_r - \omega_n) \right\}_{k=(\alpha,0,1)} dt,$$

$$M_3 = \int_{-\infty}^{+\infty} \sin t \operatorname{Re} \left\{ i|k|^{-2} \varepsilon_{1mn} k_m (i|k|^{-2} \varepsilon_{nsr} k_s \omega_r - \omega_n) \right\}_{k=(\alpha,0,1)} dt,$$

$$M_4 = \int_{-\infty}^{+\infty} \sum_k \operatorname{Re} \left\{ i|k|^{-2} \varepsilon_{1mn} k_m (i|k|^{-2} \varepsilon_{nsr} k_s \omega_r - \omega_n) \right\} dt,$$

where the sum is over the Galerkin truncation, all the integrals are evaluated along the lower heteroclinic orbit in Figure 35 for the time interval $[-29.33/2, 29.33/2]$, rather than $(-\infty, \infty)$. Direct numerical computation gives that

$$M_1 = 645.7, \quad M_2 = 1.581, \quad M_3 = 0, \quad M_4 = 47.86.$$

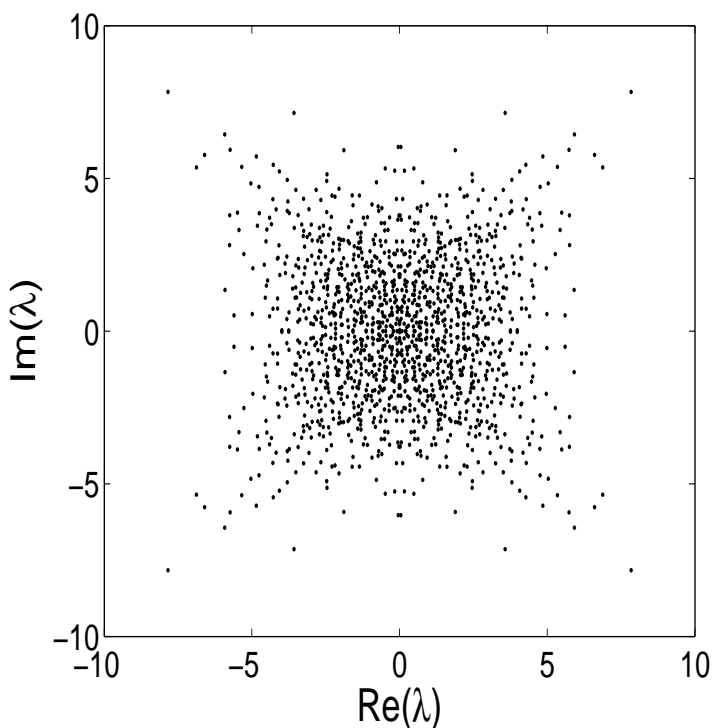


FIGURE 34. The eigenvalues of the (Galerkin truncation of) linear NS at the ABC flow when $\epsilon = 0$.

When $b = 0$ (no control), M has roots when

$$|a| > 408.4 .$$

When $\epsilon = 10^{-5}$, $b = 0$, and $T = 4 \times 10^4 \pi$, we find that

$a = 300$	$a = 400$	$a = 420$	$a = 600$	$a = 800$
$\sigma = 0.8 \times 10^{-5}$	$\sigma = 1.3 \times 10^{-4}$	$\sigma = 0.8 \times 10^{-4}$	$\sigma = 4.9 \times 10^{-4}$	$\sigma = 4.9 \times 10^{-4}$

Around $a = 400$, σ has a jump of one order which seems to be in agreement with the Melnikov prediction. However, when $a = 100$, $\sigma = 3.6 \times 10^{-4}$ which shows that the Melnikov prediction is not very effective. We do not know the specific reason.

10. Melnikov Integral and Control of Chaos in 3D Navier-Stokes Equation

Now we turn on the control ($b \neq 0$). When

$$b = -M_1/M_4 \approx -13.5 ,$$

the Melnikov integral M (9.1) has roots for any a .

When $\epsilon = 10^{-5}$, $b = -13.5$, and $T = 4 \times 10^4 \pi$, we find that

$a = 1$	$a = 10$	$a = 100$	$a = 200$
$\sigma = 0.098$	$\sigma = 0.125$	$\sigma = 0.095$	$\sigma = 0.083$

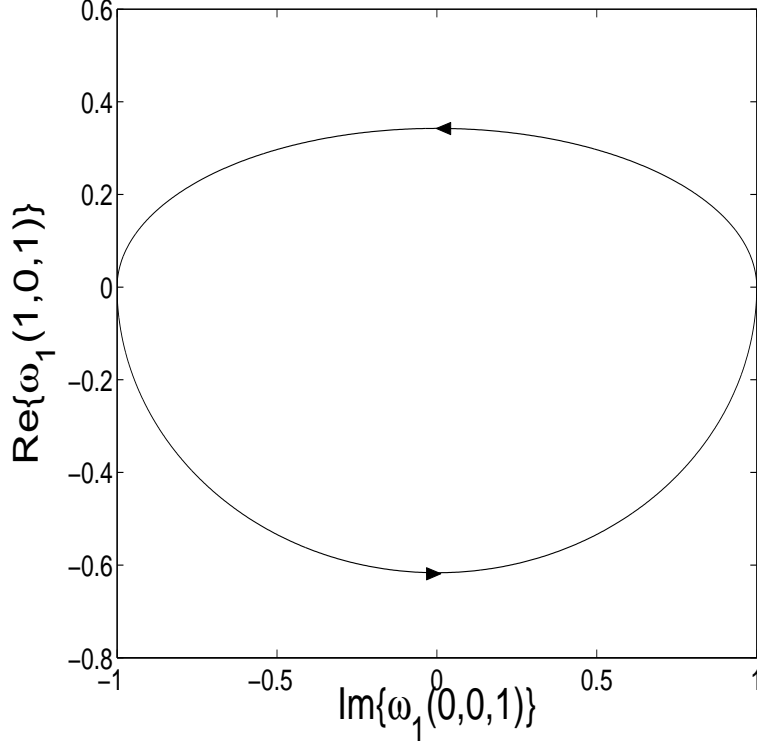


FIGURE 35. An approximate heteroclinic cycle of the Galerkin truncation: $|\kappa_n| \leq 1$ ($n = 1, 2, 3$) of the 3D Euler equations.

Thus under the control, chaos exists even when $a = 1$. Also changing the value of b, σ does not change dramatically. Therefore, our control prediction above may not be very effective.

11. Numerical Verification of the Heteroclinics Conjecture for a Line Model

Returning to the 2D Navier-Stokes equation (2.1), numerical simulations on large Galerkin truncations are still challenging to the current computer ability. Here we will study a simple line model [12] obtained by a special Galerkin truncation [12]. Let $p = (1, 0)$ and $\hat{k} = (0, \alpha)$, the line model is given by the Galerkin truncation:

$$\{\pm p, \pm(\hat{k} + np), \quad \forall n \in \mathbb{Z}\}$$

We will work in the invariant subspace where ω_k 's are real-valued. The governing equation of the line model is

$$(11.1) \quad \begin{aligned} \dot{\omega}_n &= A_{n-1}\omega_*\omega_{n-1} - A_{n+1}\omega_*\omega_{n+1} \\ &+ \epsilon[-(n^2 + \alpha^2)\omega_n + F_n + b\Delta_n], \end{aligned}$$

$$(11.2) \quad \dot{\omega}_* = -\sum_{n \in \mathbb{Z}} A_{n-1,n}\omega_{n-1}\omega_n + \epsilon[-\omega_* + F_* + b\Delta_*],$$

where $\omega_n = \omega_{\hat{k}+np}$, $\omega_* = \omega_p$, similarly for F and Δ as the Fourier transforms of f and $\tilde{\delta}$, and

$$A_n = 2A(p, \hat{k} + np) = \alpha \left[\frac{1}{n^2 + \alpha^2} - 1 \right] ,$$

$$A_{n-1,n} = 2A(\hat{k} + (n-1)p, \hat{k} + np) = \alpha \left[\frac{1}{(n-1)^2 + \alpha^2} - \frac{1}{n^2 + \alpha^2} \right] .$$

For the line model, verification of the heteroclinics conjecture is relatively easier. First of all, for the line model ($\epsilon = 0$), it can be proved that the fixed point $\Omega = 2 \cos x_1$ has a 1-dimensional local unstable manifold W^u . The basic idea of the proof is that one can apply the Riesz projections to the spectrum of the linearized line model operator at the fixed point, and the nonlinear terms have bounded coefficients so that they are quadratic in a Banach algebra. For the full 2D Euler equation, the difficulty lies at the fact that the nonlinear term is not quadratic in a Banach algebra.

Denote by Σ the 1 co-dimensional hyperplane

$$\Sigma = \{ \omega \mid \omega_{(1,0)} = 0 \} .$$

We have the corollary of Theorem 3.1.

Corollary 11.1. *Assume that $W^u \cap \Sigma \neq \emptyset$; then the heteroclinics conjecture is true, i.e. there is a heteroclinic orbit that connects $\Omega = 2 \cos x_1$ and $-\Omega$.*

For any truncation ($|n| \leq N$) of the line model, we first calculate the unstable eigenvector. Then we track the heteroclinic orbit with the initial condition provided by the unstable eigenvector. Numerically exact heteroclinic orbit is obtained for any N ($|n| \leq N$). That is, for any N ($|n| \leq N$), it can be verified numerically that

$$W^u \cap \Sigma \neq \emptyset .$$

For $|n| \leq 32$, the heteroclinic orbit is shown in Figure 36. In comparison with the full 2D Euler equation, the hyperplane Σ here is only 1 co-dimensional. This is the simplest nontrivial case to study the intersection $W^u \cap \Sigma$. We also conduct calculations on the Liapunov exponents. When $\epsilon = 0$, $|n| \leq 32$, $\sigma = 0$ for all the computed time intervals, which means that there is no chaos. This is true for any N ($n \leq N$) and any computational time interval. This indicates that the line model may be integrable when $\epsilon = 0$. From these facts, it is clear that the line model is a good starting point for a rigorous analysis. For instance, it is hopeful to make the Melnikov integral theory rigorous.

12. Melnikov Integral and Numerical Simulation of Chaos in the Line Model

For the line model, the kinetic energy and enstrophy are still invariants when $\epsilon = 0$. Choosing the same external force (5.1) and control (6.1), we have the Melnikov integral which is the same with that of 2D NS except that the Fourier modes summation is over the line model,

$$(12.1) \quad M_0 = M_1 + a \sqrt{M_2^2 + M_3^2} \sin(t_0 + \theta) + b M_c .$$

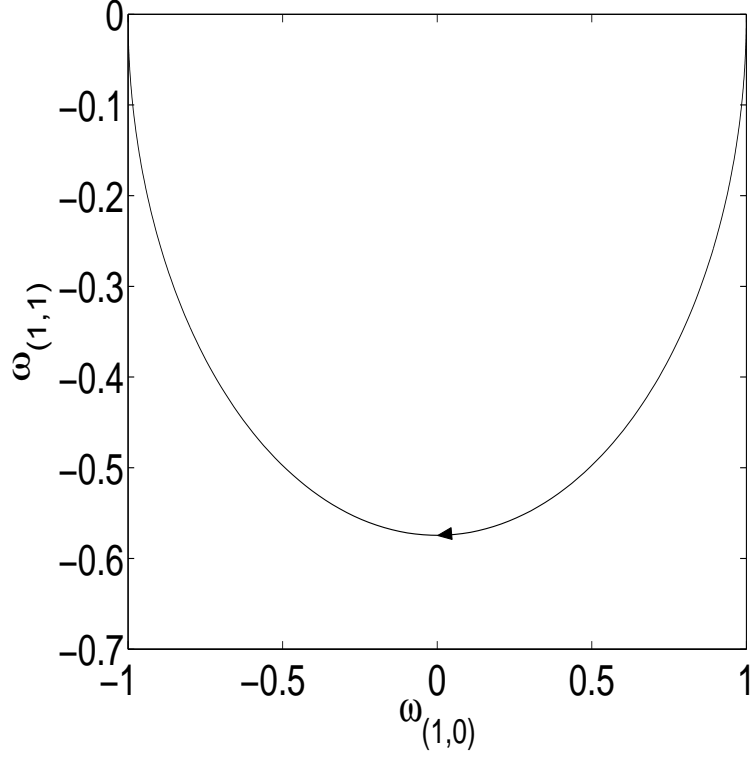


FIGURE 36. Numerically exact heteroclinic orbit of the line model ($\epsilon = 0$) for $|n| \leq 32$.

For the truncation $|n| \leq 32$, we evaluate these integrals along the heteroclinic orbit in Figure 36, and obtain that

$$M_1 = -6.0705, \quad M_2 = -0.10665, \quad M_3 = 0, \quad M_c = 11.9728$$

For the case of no control ($b = 0$), when

$$|a| > 56.92$$

the Melnikov integral M has roots.

We conduct some numerical simulations on the (transient) chaos. When $\epsilon = 10^{-3}$, and $T = 2 \times 10^3 \pi$, we find that

$$\begin{array}{ll} a \leq 200 & a = 400 \\ \sigma < 0 & \sigma = 7.2 \times 10^{-4} . \end{array}$$

According to the roots of the Melnikov integral, when $|a| > 56.92$, the broken heteroclinic orbit may re-intersect with certain center-stable manifold. According the above Liapunov exponent result, transient chaos is generated when $a = 400$ which may be due to the generation of new heteroclinic cycles. As can be expected, the Melnikov prediction performs better here for the line model. When $\epsilon = 0$, there is no chaos. When $\epsilon > 0$, we see that transient chaos appears when $|a|$ is greater than certain threshold which is in the range $|a| > 56.92$ predicted by the Melnikov integral.

13. Melnikov Integral and Control of Chaos in the Line Model

Now we turn on the control ($b \neq 0$). When

$$b = -M_1/M_c = 0.50702425$$

the Melnikov integral M has roots for any a . To test the effectiveness of the control, we set b to the above value and conduct some numerical simulations on the (transient) chaos. When $\epsilon = 10^{-3}$, $b = 0.50702425$, and $T = 2 \times 10^3\pi$, we find that

$$\begin{array}{ccccc} a = 1 & a = 10 & a = 50 & a = 200 & a = 400 \\ \sigma = -12.6 \times 10^{-4} & \sigma = 2 \times 10^{-4} & \sigma = 0.2 \times 10^{-4} & \sigma = 2 \times 10^{-4} & \sigma = 0.87 \times 10^{-4} . \end{array}$$

The control clearly enhanced the transient chaos. The control effectively pushed the threshold of a backward from 400 to 10 for the generation of transient chaos. This shows that the Melnikov integral control performs better here for the line model.

14. Numerical Verification of the Heteroclinics Conjecture for a Two Lines Model

To gain an understanding of the effect of the other modes np ($|n| \geq 2$) on the line model, we introduce the two lines model which is the Galerkin truncation:

$$\{(k_1, k_2), \quad |k_2| \leq 1\}.$$

We also work in the invariant subspace where ω_k 's are real-valued.

For the two lines model, one can derive the governing equations in the physical variables. Let

$$\Omega = \omega(t, x) + e^{i\alpha y} q(t, x) + e^{-i\alpha y} \bar{q}(t, x) ,$$

where ω is real-valued, q is complex-valued (the Fourier transform of q is real-valued), and

$$\int_0^{2\pi} \omega(t, x) dx = 0 .$$

Let

$$f + b\tilde{\delta} = \eta(t, x) + e^{i\alpha y} F(t, x) + e^{-i\alpha y} \bar{F}(t, x) ,$$

where η is real-valued, F is complex-valued (the Fourier transform of F is real-valued), and

$$\int_0^{2\pi} \eta(t, x) dx = 0 .$$

Substituting the above expressions into the 2D NS (2.1), and ignoring the terms involving $e^{i2\alpha y}$ and $e^{-i2\alpha y}$, one gets the two lines model in the physical variables,

$$(14.1) \quad i\partial_t q + \alpha [(\partial_x \omega)(\partial_x^2 - \alpha^2)^{-1} - (\partial_x^{-1} \omega)] q = i\epsilon [(\partial_x^2 - \alpha^2)q + F] ,$$

$$(14.2) \quad \partial_t \omega + i\alpha \partial_x [q(\partial_x^2 - \alpha^2)^{-1} \bar{q} - \bar{q}(\partial_x^2 - \alpha^2)^{-1} q] = \epsilon [\partial_x^2 \omega + \eta] .$$

Introducing $\theta = \partial_x^{-1} \omega$, $\varphi = (\partial_x^2 - \alpha^2)^{-1} q$, and $h = \partial_x^{-1} \eta$, one gets

$$(14.3) \quad i\partial_t q + \alpha(\varphi \partial_x^2 \theta - \theta q) = i\epsilon [(\partial_x^2 - \alpha^2)q + F] ,$$

$$(14.4) \quad \partial_t \theta + i\alpha(q\bar{\varphi} - \bar{q}\varphi) = \epsilon [\partial_x^2 \theta + h] ,$$

$$(14.5) \quad (\partial_x^2 - \alpha^2)\varphi = q .$$

When $\epsilon = 0$, then Kinetic energy and enstrophy

$$E_0 = \int_0^{2\pi} [\theta^2 + 2\alpha^2|\varphi|^2 + 2|\partial_x\varphi|^2] dx, \quad E_1 = \int_0^{2\pi} [\omega^2 + 2|q|^2] dx,$$

are still invariants.

Denote by Σ the hyperplane

$$\Sigma = \{\omega \mid \omega_k = 0, \quad \text{whenever } k_2 = 0\}.$$

For the two lines model, when $\epsilon = 0$, existence of a local unstable manifold for the fixed point $\Omega = 2 \cos x_1$ is an open problem due to the fact that the coefficients of the nonlinear terms are not bounded, i.e. the nonlinear terms are not quadratic in a Banach algebra. Then we have the corollary of Theorem 3.1.

Corollary 14.1. *Assume that the fixed point $\Omega = 2 \cos x_1$ has a 1-dimensional local unstable manifold W^u , and $W^u \cap \Sigma \neq \emptyset$; then the heteroclinics conjecture is true, i.e. there is a heteroclinic orbit that connects $\Omega = 2 \cos x_1$ and $-\Omega$.*

For any truncation ($|k_1| \leq N$) of the two lines model, we first calculate the unstable eigenvector. Then we track the heteroclinic orbit with the initial condition provided by the unstable eigenvector. For $|k_1| \leq 2$, numerically exact heteroclinic orbit is obtained. That is, it can be verified numerically that

$$W^u \cap \Sigma \neq \emptyset.$$

Figure 37 shows the numerically exact heteroclinic orbit. For $|k_1| \leq 4$,

$$\text{Distance}(W^u, \Sigma) \approx 0.0086.$$

Figure 38 shows the approximate heteroclinic orbit. For $|k_1| \leq 16$,

$$\text{Distance}(W^u, \Sigma) \approx 0.012.$$

Figure 39 shows the corresponding approximate heteroclinic orbit. Unlike the line model, here we do not always get numerically exact heteroclinic orbits. This is due to the influence of the modes $(k_1, 0)$.

15. Melnikov Integral and Numerical Simulation of Chaos in the Two Lines Model

When $\epsilon = 0$, there is very weak chaos for the computational interval $t \in [0, 4 \times 10^4 \pi]$:

$$\begin{array}{ccc} |n| \leq 4 & |n| \leq 8 & |n| \leq 16 \\ \sigma = 9.5 \times 10^{-4} & \sigma = 8.2 \times 10^{-4} & \sigma = 8.5 \times 10^{-4}. \end{array}$$

For the two lines model, the kinetic energy and enstrophy are still invariants when $\epsilon = 0$. Choosing the same external force (5.1) and control (6.1), we have the Melnikov integral which is the same with that of 2D NS except that the Fourier modes summation is over the two lines model,

$$(15.1) \quad M_0 = M_1 + a\sqrt{M_2^2 + M_3^2} \sin(t_0 + \theta) + bM_c.$$

For the truncation $|k_1| \leq 16$, we evaluate these integrals along the heteroclinic orbit in Figure 39, and obtain that

$$M_1 = -4.9, \quad M_2 = -0.0948, \quad M_3 = 0, \quad M_c = 12.2498.$$

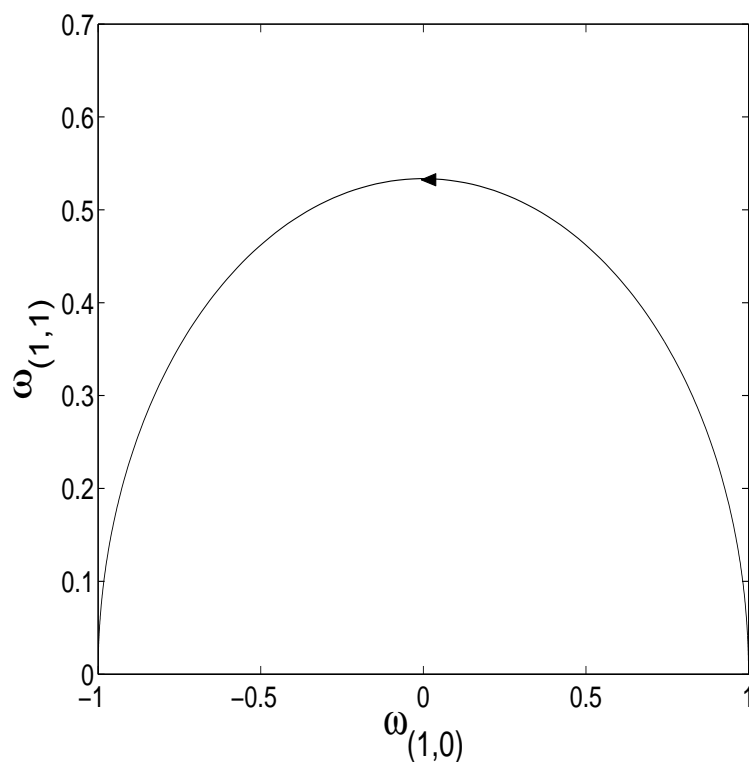


FIGURE 37. Numerically exact heteroclinic orbit of the two lines model for $|k_1| \leq 2$.

For the case of no control ($b = 0$), when

$$|a| > 51.688 ,$$

the Melnikov integral M has roots. We conduct some numerical simulations on the (transient) chaos. When $\epsilon = 10^{-3}$, and $T = 2 \times 10^3 \pi$, we find that

$$\begin{aligned} a &\leq 200 & a &= 400 \\ \sigma &< 0 & \sigma &= 1.27 \times 10^{-2} . \end{aligned}$$

According to the roots of the Melnikov integral, when $|a| > 51.688$, the broken heteroclinic orbit may re-intersect with certain center-stable manifold. According to the above Liapunov exponent result, strong transient chaos is generated when $a = 400$ which may be due to the generation of new heteroclinic cycles. Thus the result is almost the same as that of the line model. As can be expected, the Melnikov prediction also performs well here for the two lines model. When $\epsilon = 0$, there is weak transient chaos. When $\epsilon > 0$, we see that strong transient chaos appears when $|a|$ is greater than certain threshold which is in the range $|a| > 51.688$ predicted by the Melnikov integral. In comparison with the line model, here the transient chaos seems very strong. On the other hand, when $\epsilon = 0$, the two lines model here still has weak chaos, in contrast to the fact of no chaos at all for the line model.

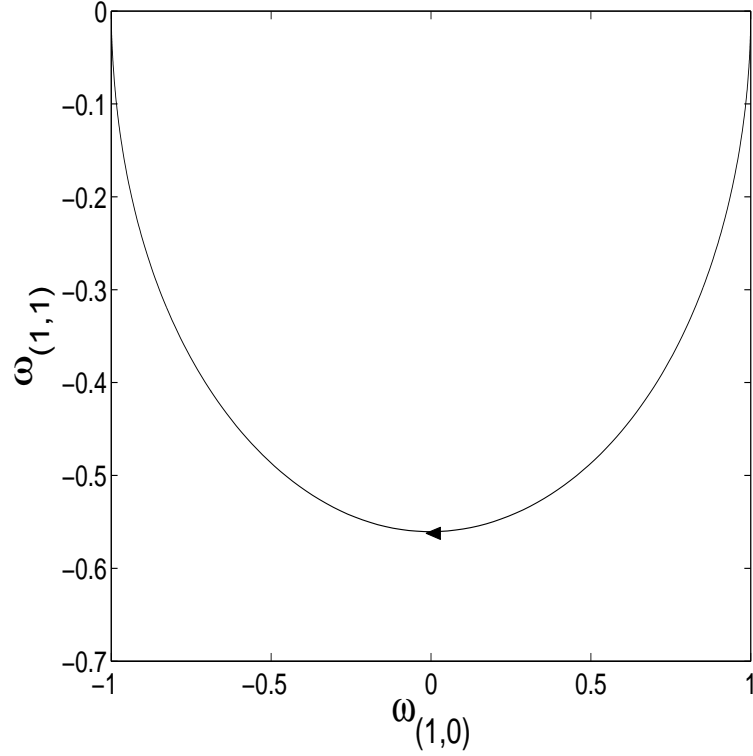


FIGURE 38. Approximate heteroclinic orbit of the two lines model for $|k_1| \leq 4$.

16. Melnikov Integral and Control of Chaos in the Two Lines Model

Now we turn on the control ($b \neq 0$). When

$$b = -M_1/M_c = 0.4 ,$$

the Melnikov integral M has roots for any a . To test the effectiveness of the control, we set b to the above value and conduct some numerical simulations on the (transient) chaos. When $\epsilon = 10^{-3}$, $b = 0.4$, and $T = 2 \times 10^3 \pi$, we find that

$$\begin{array}{ccccc} a \leq 400 & a = 500 & a = 600 & a = 700 & a = 800 \\ \sigma < 0 & \sigma = 0.97 \times 10^{-3} & \sigma = 3.0 \times 10^{-4} & \sigma = 4.6 \times 10^{-2} & \sigma = 5.0 \times 10^{-2} . \end{array}$$

The control seems to tame the transient chaos, in contrast to the line model. The control pushed the threshold of a forward from 400 to 700 for the generation of strong transient chaos.

17. Conclusion and Discussion

Through a combination of analytical and numerical studies, we now have a better understanding on the zero viscosity limit of the spectra of linear NS operators. We proposed and numerically studied the so-called heteroclinics conjecture for both 2D and 3D Euler equations. We also proposed the Melnikov integral as a tool for predicting and controlling chaos.

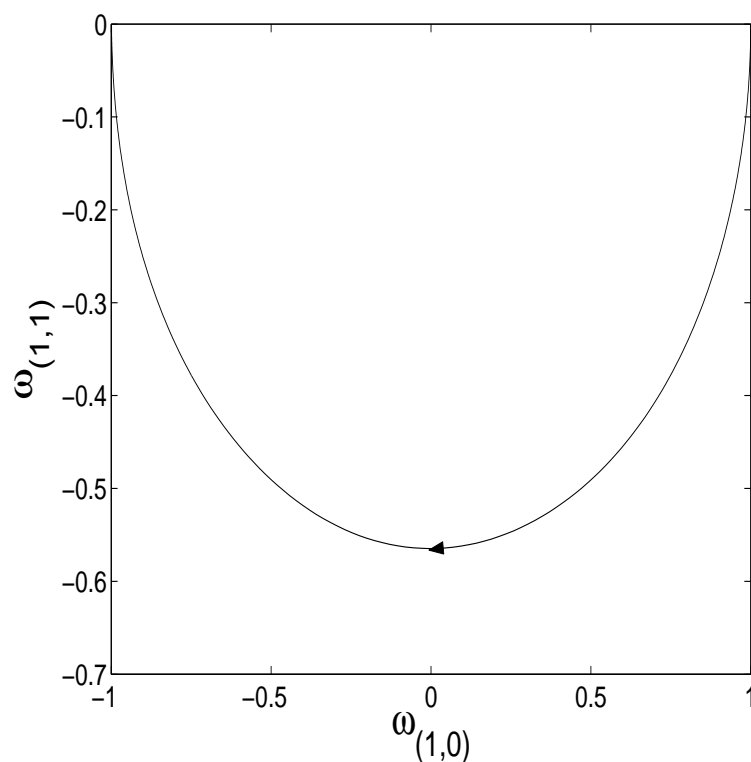


FIGURE 39. Approximate heteroclinic orbit of the two lines model for $|k_1| \leq 16$.

Our numerical verification on the heteroclinics conjecture was limited by reasonable computing time. We realized that increasing the size of the Galerkin truncations can quickly reach the limit of our computer ability. We did not try to utilize today's supercomputer due to the fact that Galerkin truncations are essentially singular perturbations of Euler equations. We believe that analysis is the key to a better understanding of the heteroclinics conjecture.

We realized through our numerical simulations that Liapunov exponent performs very well as a measure of (even transient) chaos. Our Melnikov prediction for NS equations is of course not as rigorous and effective as that for sine-Gordon system. In fact, it is a rough indicator for predicting and controlling chaos. Nevertheless, we believe that the Melnikov integral theory for NS equations has a lot of potential especially in the current circumstance that there is no effective tools dealing with chaos in NS equations.

We also believe that both the line and the two lines models have great potential in future analytical studies on modeling the dynamics of 2D NS equations.

18. Appendix A: Melnikov Integral and Control of Chaos in a Sine-Gordon Equation

Consider the sine-Gordon equation [15]

$$(18.1) \quad u_{tt} = \frac{9}{16}u_{xx} + \sin u + \epsilon \left[-au_t + \left(1 + b\tilde{\delta}(x)\right) \cos t \sin^3 u \right],$$

which is subject to periodic boundary condition and odd constraint

$$(18.2) \quad u(t, x + 2\pi) = u(t, x), \quad u(t, -x) = -u(t, x),$$

where u is a real-valued function of two real variables (t, x) , ϵ is a small perturbation parameter, $a > 0$ is the damping coefficient, $b\tilde{\delta}(x)$ is the spatially localized control, $\tilde{\delta}(x)$ is an even and 2π -periodic function of x , and b is the control parameter. The system (18.1) is invariant under the transform $u \rightarrow -u$.

The natural phase space for (18.1) is $(u, u_t) \in H^{n+1} \times H^n$ ($n \geq 0$) where H^n is the Sobolev space on $[0, 2\pi]$. Let P be the Poincaré period- 2π map of (18.1) in $H^{n+1} \times H^n$. Without the control ($b = 0$), we have the following chaos theorem [15] [19].

Theorem 18.1 ([15]). *There exists a constant $a_0 > 0$, when ϵ is sufficiently small, for any $a \in [\frac{1}{100}a_0, a_0]$ there exists a symmetric pair of homoclinic orbits h_{\pm} ($h_- = -h_+$) asymptotic to $(u, u_t) = (0, 0)$. In the neighborhood of h_{\pm} , there exists chaos to the sine-Gordon equation (18.1) in the following sense: There is a Cantor set Ξ of points in $H^{n+1} \times H^n$ ($n \geq 0$), which is invariant under an iterated Poincaré period- 2π P^K for some K . The action of P^K on Ξ is topologically conjugate to the Bernoulli shift on two symbols 0 and 1.*

In the product topology, the Bernoulli shift has the property of sensitive dependence upon initial data - the signature of chaos.

When we turn on the control ($b \neq 0$), we hope to find values of b such that the chaos in Theorem 18.1 is controlled (tamed - annihilated or less chaotic, enhanced - more chaotic). Our main tool is the Melnikov function. To build such a function, we need results from integrable theory. When $\epsilon = 0$, the fixed point ($u = 0$) of the sine-Gordon equation (18.1) has a figure eight connecting to it [15]:

$$(18.3) \quad u = \pm 4 \arctan \left[\frac{\sqrt{7}}{3} \operatorname{sech} \tau \sin x \right],$$

where $\tau = \frac{\sqrt{7}}{4}(t - t_0)$ and t_0 is a real parameter. Along this figure eight, a Melnikov vector has the expression [15]:

$$(18.4) \quad \frac{\partial F_1}{\partial u_t} = \pm \frac{7\pi}{12\sqrt{2}} \operatorname{sech} \tau \tanh \tau \sin x \left[\frac{9}{16} + \frac{7}{16} \operatorname{sech}^2 \tau \sin^2 x \right]^{-1},$$

where F_1 is a constant of motion. When $\epsilon \neq 0$, the Melnikov function for (18.1) is given by [15]:

$$M(t_0, a, b) = \int_{-\infty}^{+\infty} \int_0^{2\pi} \frac{\partial F_1}{\partial u_t} \left[-au_t + \left(1 + b\tilde{\delta}(x)\right) \cos t \sin^3 u \right] dx dt,$$

where u and $\frac{\partial F_1}{\partial u_t}$ are given in (18.3) and (18.4). Using the odd and even property of (18.3) and (18.4) in t and x , we obtain

$$(18.5) \quad M(t_0, a, b) = -aM_a + \sin t_0 (M_0 + bM_b),$$

where

$$\begin{aligned} M_a &= \int_{-\infty}^{+\infty} \int_0^{2\pi} \frac{\partial F_1}{\partial u_t} u_t \, dx dt , \\ M_0 &= - \int_{-\infty}^{+\infty} \int_0^{2\pi} \frac{\partial F_1}{\partial u_t} \sin \frac{4}{\sqrt{7}} \tau \sin^3 u \, dx dt , \\ M_b &= - \int_{-\infty}^{+\infty} \int_0^{2\pi} \frac{\partial F_1}{\partial u_t} \tilde{\delta}(x) \sin \frac{4}{\sqrt{7}} \tau \sin^3 u \, dx dt . \end{aligned}$$

In the phase space $H^{n+1} \times H^n$ ($n \geq 0$), $(u, u_t) = (0, 0)$ is a saddle point under the Poincaré period- 2π map of (18.1) with one-dimensional unstable manifold W^u and one-codimensional stable manifold W^s . The Melnikov function $\epsilon M(t_0, a, b)$ is the leading order term of the distance between W^u and W^s . For the entire rigorous theory, see [16]. When $|aM_a| < |M_0 + bM_b|$, the roots of M are given by

$$(18.6) \quad \sin t_0 = \frac{aM_a}{M_0 + bM_b} .$$

Near these roots, W^u and W^s intersect. This leads to the existence of a symmetric pair of homoclinic orbits and chaos in Theorem 18.1. When $|aM_a| > |M_0 + bM_b|$, i.e.

$$(18.7) \quad -a|M_a| - M_0 < bM_b < a|M_a| - M_0 ,$$

the Melnikov function is not zero, and we have the following theorem.

Theorem 18.2. *When the control parameter b satisfies (18.7), the chaos in Theorem 18.1 disappears.*

PROOF. When the control parameter b satisfies (18.7), the Melnikov function is not zero for any t_0 , and W^u and W^s do not intersect. Thus the pair of homoclinic orbits and the corresponding chaos in Theorem 18.1 disappear. \square

Theorem 18.2 only claims that the chaos in Theorem 18.1 disappears. This does not mean that there is no chaos in the entire phase space $H^{n+1} \times H^n$ ($n \geq 0$). An important point here is that by manipulating the localized control $b\tilde{\delta}(x)$, one can change the Melnikov function which leads to the disappearance of the non-localized (in x) chaos. The control condition (18.7) is also interesting: It is not true that the larger the control parameter b is, the better the taming is. In fact, when b is large enough, the chaos will reappear.

When $|aM_a| < |M_0 + bM_b|$, the Melnikov function (18.5) has roots (18.6), and Theorem 18.1 holds. As a function of t_0 , the Melnikov function M has the maximal absolute value (the L^∞ norm),

$$M_*(a, b) = a|M_a| + |M_0 + bM_b| ,$$

for $t_0 \in [0, 2\pi]$. M_* is the leading order term of the maximal distance between W^u and W^s . Notice that W^u and W^s intersects near the t_0 given by (18.6). So the larger the M_* is, the more violent the chaos is. Thus $M_*(a, b)$ serves as a measure of the strength of the chaos. By changing the control parameter b , we can adjust the strength M_* of the chaos - enhancing or decreasing.

19. Appendix B: The Lagrange Flow Induced by a Solution to the 2D Euler Equation Is Always Integrable

It is well-known that 2D Euler equation is globally well-posed [5] [6]. For any solution to the 2D Euler equation, let $\Psi = \Psi(t, x_1, x_2)$ be the corresponding stream function. Then the Lagrange flow induced by the solution is given by

$$(19.1) \quad \frac{dx_1}{dt} = -\frac{\partial\Psi}{\partial x_2}, \quad \frac{dx_2}{dt} = \frac{\partial\Psi}{\partial x_1}.$$

Theorem 19.1. *The Lagrange flow (19.1) induced by a solution to the 2D Euler equation is always integrable.*

PROOF. Assume that $\Psi(t, x_1, x_2)$ is not a steady state, i.e. it depends upon t (in this case $\Delta\Psi$ is functionally independent of Ψ , otherwise, $\Psi(t, x_1, x_2)$ would be a steady state). Introducing the new Hamiltonian $H = \Psi(\theta, x_1, x_2) - \psi$, and converting (19.1) into an autonomous system

$$(19.2) \quad \frac{dx_1}{dt} = -\frac{\partial H}{\partial x_2}, \quad \frac{dx_2}{dt} = \frac{\partial H}{\partial x_1}, \quad \frac{d\theta}{dt} = -\frac{\partial H}{\partial \psi}, \quad \frac{d\psi}{dt} = \frac{\partial H}{\partial \theta}.$$

Notice that the vorticity $\Omega = \Delta\Psi$ is another constant of motion of (19.2) besides H :

$$\frac{d}{dt}\Delta\Psi = \partial_\theta\Delta\Psi - \partial_{x_1}\Delta\Psi\partial_{x_2}\Psi + \partial_{x_2}\Delta\Psi\partial_{x_1}\Psi = 0.$$

Since $\Delta\Psi$ is independent of ψ , $\Delta\Psi$ and H are functionally independent. Thus (19.2) is integrable in the Liouville sense. In the case that Ψ is independent of t (i.e. a steady state), then (19.1) is an autonomous system, thus also integrable in the Liouville sense. \square

A common way to obtain steady states of 2D Euler equation is by solving

$$\Delta\Psi = f(\Psi)$$

where $f(\Psi)$ is an arbitrary function of Ψ , i.e. $\Delta\Psi$ and Ψ are functionally dependent.

References

- [1] N. Alexeeva, et al., Taming spatiotemporal chaos by impurities in the parametrically driven nonlinear Schrödinger equation, *J. Nonlinear Math. Phys.* **8**, suppl. (2001), 5-12.
- [2] T. Dombre, et al., Chaotic streamlines in the ABC flows, *J. Fluid Mech.* **167** (1986), 353-391.
- [3] F. Feudel, N. Seehafer, On the bifurcation phenomena in truncations of the 2D Navier-Stokes equations, *Chaos Solitons Fractals* **5**, no.10 (1995), 1805-1816.
- [4] F. Feudel, N. Seehafer, Bifurcations and pattern formation in a two-dimensional Navier-Stokes fluid, *Phys. Rev. E* **52**, no.4 (1995), 3506-3511.
- [5] T. Kato, Quasi-linear equations of evolution, with applications to partial differential equations, *Lecture Notes in Mathematics* **448** (1975), 25-70.
- [6] T. Kato, Remarks on the Euler and Navier-Stokes equations in \mathbb{R}^2 , *Proc. Symp. Pure Math., Part 2* **45** (1986), 1-7.
- [7] G. Kawahara, S. Kida, Periodic motion embedded in plane Couette turbulence: regeneration cycle and burst, *J. Fluid Mech.* **449** (2001), 291-300.
- [8] J. Kim, Control of turbulent boundary layers, *Physics of Fluids* **15**, no.5 (2003), 1093-1105.
- [9] Y. Latushkin, Y. Li, M. Stanislavova, The spectrum of a linearized 2D Euler operator, *Studies in Appl. Math.* **112** (2004), 259-270.
- [10] Y. Li, On 2D Euler equations: Part I. On the energy-Casimir stabilities and the spectra for linearized 2D Euler equations, *J. Math. Phys.* **41**, no.2 (2000), 728-758.
- [11] Y. Li, A Lax pair for 2D Euler equation, *J. Math. Phys.* **42**, No.8 (2001), 3552-3553.
- [12] Y. Li, On 2D Euler equations: Part II. Lax pairs and homoclinic structures, *Comm. on Appl. Nonlinear Analysis* **10**, no.1 (2003), 1-43.

- [13] Y. Li, Chaos and shadowing lemma for autonomous systems of infinite dimensions, *J. Dynam. Diff. Eq.* **15** (2003), 699-730.
- [14] Y. Li, Chaos and shadowing around a homoclinic tube, *Abstr. Appl. Anal.* **2003**, no. **16** (2003), 923-931.
- [15] Y. Li, Homoclinic tubes and chaos in perturbed sine-Gordon equation, *Chaos Solitons Fractals* **20**, no. **4** (2004), 791-798.
- [16] Y. Li, *Chaos in Partial Differential Equations*, International Press, Somerville, MA, USA, (2004).
- [17] Y. Li, Invariant manifolds and their zero-viscosity limits for Navier-Stokes equations, *Dynamics of PDE* **2**, no. **2** (2005), 159-186.
- [18] Y. Li, Zero dispersion and viscosity limits of invariant manifolds for focusing nonlinear Schrödinger equations, *J. Math. Anal. Appl.* **315** (2006), 642-655.
- [19] Y. Li, Chaos and shadowing around a heteroclinically tubular cycle with an application to sine-Gordon equation, *Studies in Appl. Math.* **116** (2006), 145-171.
- [20] Y. Li, Ergodic isospectral theory of the Lax pairs of Euler equations with harmonic analysis flavor, *Proc. Amer. Math. Soc.* **133** (2005), 2681-2687.
- [21] Y. Li, On the true nature of turbulence, *The Mathematical Intelligencer*, in press (2006).
- [22] Y. Li, Chaos in wave interactions, *Intl. J. Bifurc. Chaos*, in press (2006).
- [23] Y. Li, A. Yurov, Lax pairs and Darboux transformations for Euler equations, *Studies in Appl. Math.* **111** (2003), 101-113.
- [24] C. Lin, On the stability of two-dimensional parallel flows, *Quarterly of Appl. Math.* **3** (1945-1946), 117-142, 218-234, 277-301.
- [25] J. Lumley, P. Blossey, Control of turbulence, *Annu. Rev. Fluid Mech.* **30** (1998), 311-327.
- [26] D. Molenaar, H. Clercx, G. van Heijst, Transition to chaos in a confined two-dimensional fluid flow, *Phys. Rev. Lett.* **95** (2005), 104503.
- [27] E. Otto, C. Grebogi, J. Yorke, Controlling chaos, *Phys. Rev. Lett.* **64** (1990), 1196-1199.
- [28] R. Shvydkoy, The essential spectrum of advective equations, *Preprint* (2006).
- [29] R. Shvydkoy, Y. Latushkin, The essential spectrum of the linearized 2D Euler operator is a vertical band, *Contemp. Math.* **327** (2003), 299-304.
- [30] J. Skufca, J. Yorke, B. Eckhardt, Edge of chaos in a parallel shear flow, *Phys. Rev. Lett.* **96** (2006), 174101.
- [31] Y. Tsang, E. Ott, T. Antonsen, P. Guzdar, Intermittency in two-dimensional turbulence with drag, *Phys. Rev. E.* **71** (2005), 066313.

DEPARTMENT OF CHEMISTRY, UNIVERSITY OF NORTH CAROLINA, CHAPEL HILL, NC 27599-3290 USA

E-mail address: ylan@email.unc.edu

DEPARTMENT OF MATHEMATICS, UNIVERSITY OF MISSOURI, COLUMBIA, MO 65211, USA

E-mail address: cli@math.missouri.edu